EFFECT OF STRENGTH, LOAD RATIO AND ENVIRONMENT ON NEAR-THRESHOLD FATIGUE CRACK PROPAGATION OF 2 1/4 Cr - 1 Mo STEEL.

by

GERALD FRANK ZAMISKI

B.S., SOUTHERN ILLINOIS UNIVERSITY
(1978)

SUBMITTED IN PARTIAL FULFILLMENT
OF THE REQUIREMENTS FOR THE
DEGREE OF

MASTER OF SCIENCE

at the

MASSACHUSETTS INSTITUTE OF TECHNOLOGY

August 1980

Signature of Author.....
Department of Mechanical Engineering, July 4, 1980

Certified by.....
Thesis Supervisor

Accepted by.....
Chairman, Department Committee

EFFECT OF STRENGTH, LOAD RATIO AND ENVIRONMENT ON NEAR-THRESHOLD FATIGUE CRACK PROPAGATION OF 2 1/4 Cr - 1Mo STEEL

by

GERALD F. ZAMISKI

Submitted to the Department of Mechanical Engineering on July 4, 1980 in partial fulfillment of the requirements for the degree of Master of Science.

ABSTRACT

Near-threshold fatigue crack propagation has been examined for a 2 1/4 Cr - 1 Mo quenched and tempered steel - SA542 class 2. The effects of material strength, load ratio and environment were investigated. Tests were conducted at ambient temperature in a newly constructed environmental chamber system with a design impurity level of 1 ppm. Environments consisted of moist air, and dehumidified/purified hydrogen and helium gases. Near-threshold growth was found to be dependent on material strength and load ratio. Near-threshold growth rates were enhanced in hydrogen and helium relative to moist air. Fractography displayed fracture mechanism dependence on stress intensity, load ratio and environment. The results are rationalized in terms of a crack closure model involving enlarged oxide debris formed upon near-threshold cracks. Such models are shown to be at least qualitatively consistent with experimental observations.

Thesis Supervisor: Robert O. Ritchie
Title: Associate Professor of Mechanical Engineering

ACKNOWLEDGEMENTS

I would like to sincerely thank Prof. Ritchie for his support, friendship, and for the opportunity to work for someone whose high standards and goals are reflected in his current status in the fatigue field. My respect for him is richly deserved. Never ending thanks and love to Edward, Florence, David and Terry Zamiski, for without them I may have never achieved this, my proudest moment. Also to Jeff, Sandra, Janet, Mark, Rosendo, Finis, John, Suresh, Chip and Wink, a special thanks.

TABLE OF CONTENTS

LIST OF TABLES

LIST OF FIGURES

CHAPTER I

INTRODUCTION

1.1 Review of Fatigue

In applications of 2 1/4 Cr - 1 Mo steels, conditions may exist where fatigue crack growth of subcritical flaws can lead to catastrophic failure. These flaws, which are below the resolution of NDT techniques (typically ~0.2mm), may propagate at seemingly immeasurable rates. But when design lifetimes are up to 30 years, these rates become very significant especially in the presence of harsh environments. The defect tolerant approach to design of critical applications, which is now widely used, is concerned with the lifetime (number of cycles) required to propagate a subcritical flaw from an assumed initial defect size (NDT limits) to a critical size. This approach has accelerated research on fatigue crack propagation characteristics of structural materials. Figure 1 is a schematic representation of a typical fatigue data curve, where the growth rate (da/dN) is plotted versus the alternating stress intensity (ΔK). The curve is divided into three regimes: the high growth regime (C) leading to final failure, the linear mid growth regime (B) and the low growth regime (A). Until recently, most research has centered on growth rates above 10^{-6} mm/cycle, corresponding to the mid (B) and upper (C) growth regimes where failure can occur in

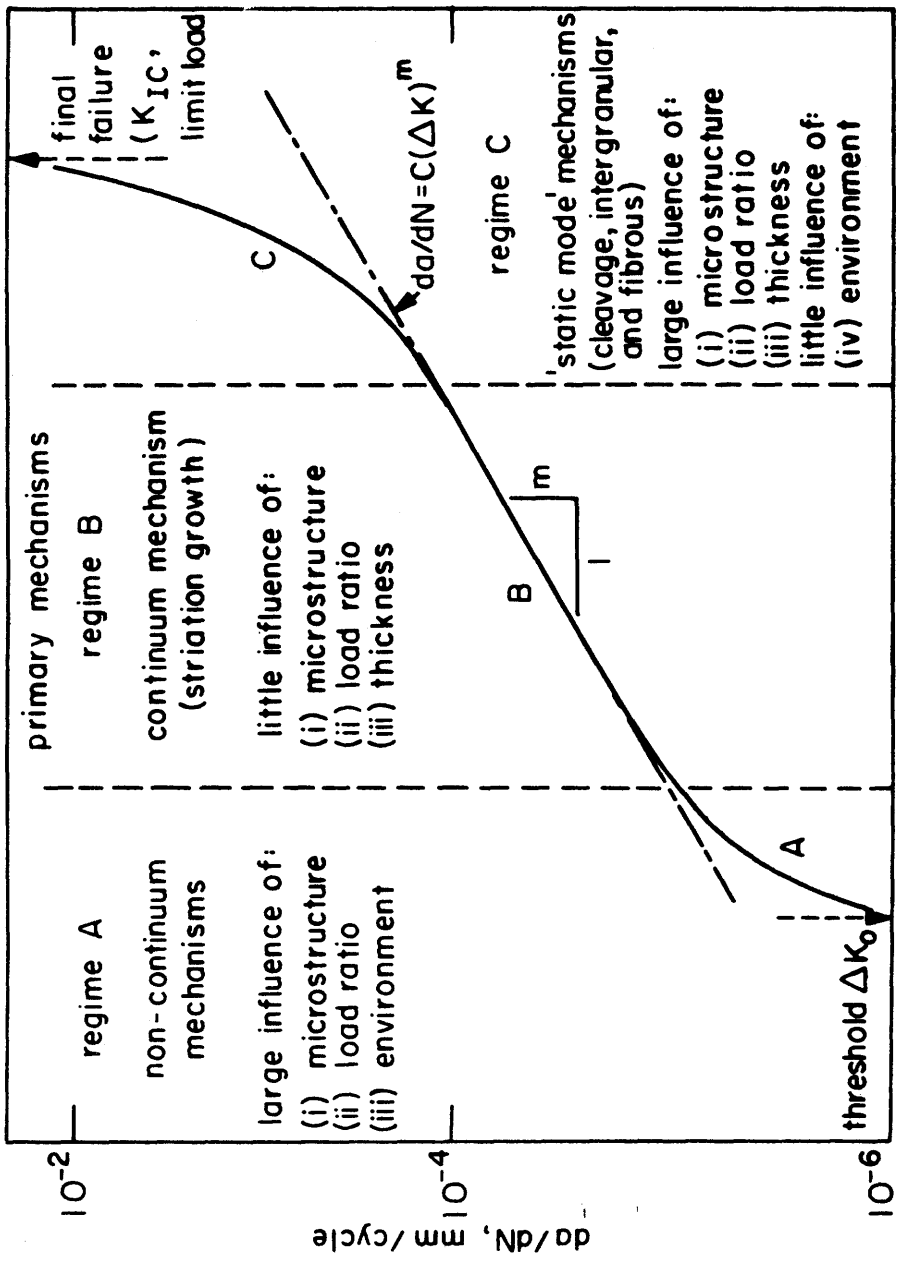

Fig. 1: Schematic of fatigue crack growth rate ($^{da}/_{dN}$) versus alternating stress intensity (ΔK) in steels.

thousands of cycles. When application design life is taken to be 10-30 years, small flaws which can be propagating at rates less than 10^{-6} mm/cycle (low growth regime A), can grow to a critical size. Consequently, research has shifted to analyzing the variables affecting this low growth regime (A), where average crack growth rates are often less than a lattice spacing per cycle. This low growth regime contains a minimum value of alternating stress intensity (ΔK) below which there is no experimentally detectable growth (less than 10^{-8} mm/cycle). This minimum value of ΔK is the threshold alternating stress intensity ΔK_o.

Studies (5, 7, 8, 19) on mid growth rates have shown that this regime is largely insensitive to changes in mean stress and microstructure. The typical failure mode of regime B is one of transgranular ductile striation (18). Regime C displays a change in fracture mode from the transgranular ductile striation to intergranular, fibrous and cleavage fracture mechanisms (19). Ritchie (5) has shown that these high growth rates are much more dependent on mean stress and microstructure.

Literature has shown that near-threshold growth rates and the value of ΔK_o are particularly dependent on mean stress or load ratio R (5, 7, 9-13, 30, 46, 56), cyclic frequency (13), yield strength (5, 12, 14), grain size (5, 15) and microstructure (5, 7, 9, 46). Cooke and Beevers (22), and others (7, 13) have shown that as the load ratio is increased, the near-threshold

growth susceptibility is also increased. Ritchie (5) and studies by Masounave and Bailon (9) show a trend of increasing near-threshold growth rates with increasing material strength. It has been found that the environment can have a significant effect on near-threshold growth, and environmentally dependent growth mechanisms have been observed (30, 46).

1.2 Objective

The objective of this study was to perform a critical analysis on the quenched and tempered 2 1/4 Cr - 1 Mo steel so as to attempt to sort out the effects of material strength, load ratio and environment on near-threshold growth in low strength steels. The analysis was directed at fully investigating the near-threshold fatigue crack growth behavior of this steel while varying pertinent application oriented conditions. The initial phase of this study consisted of laboratory heat treatment of SA542 class 2 steel over a range of tempering temperatures from 320°C to 690°C after water quenching from an austenitizing temperature of 950°C. These treatments produced a range of yield strengthes from 575 to 951 MPa. The corresponding microstructures and material properties were then examined as a function of tempering temperature. The second phase was concerned with the dependence of near-threshold fatigue growth on varying material strength. The two extreme strength conditions (320°C and 690°C) and a mid strength condition (as-received) were used as test parameters. Phase three involved

analyzing the effect of load ratio ($R = {}^{Kmin}/Kmax$) on near-threshold growth rates. Tests were conducted at a low value (R = 0.05) and a high value (R = 0.75). The fourth phase was the most pertinent as far as current near-threshold fatigue growth studies are concerned. This phase dealt with investigating the effect of strictly controlled test environments on near-threshold growth behavior. Tests were conducted at low (0.05) and high (0.75) values of R on the as-received steel (σ_{YS} = 769 MPa) in environments of moist air (30% relative humidity), highly purified and dehumidified hydrogen and helium gases. Hydrogen was chosen because it causes embrittlement of high strength steels. Vigorously purified helium gas was used in an attempt to provide an inert environment. To accomplish these purified test environments, an environmental chamber system was designed and built. Full details are given in Appendix A. The importance of these highly purified and dehumidified environments was to delineate the effect of hydrogen without oxygen, moisture and other impurities, and to produce a 'pure' inert environment. Several studies in the literature have produced contradictory results from similar environmental testing, and this has been thought to be due to varying purity of the hydrogen and inert atmospheres. The hydrogen and helium tests were both conducted at a pressure of 110 kPa, and all tests were at ambient temperature. The two extreme strength conditions (320°C and 690°C) were also tested at a

low value of R (0.05) in the same three environments. The final phase of this study involved a complete fractographic analysis using a scanning electron miscroscope. Fracture mechanisms are described as a function of yield strength, load ratio, stress intensity and environment.

Chapter II

EXPERIMENTAL PROGRAM

2.1 MATERIALS

The material tested in this program was a quenched and tempered SA542 class 2 steel of composition:

C	Mn	Si	Ni	Cr	Mo	P	S
0.14	0.44	0.22	0.61	2.28	0.92	0.01	0.02

Wei of Lehigh University supplied two 25mm thick plates of this steel measuring 320 x 660mm. These sections were originally cut from an electric furnace heat (# C7158) obtained from Lukens Steel Company. The as-received properties of SA542 class 2 have been measured by Wei and Simmons (39).

2.2 SPECIMEN GEOMETRY

Fatigue crack propagation specimens usedin this study were ASTM standard 1-T compact (CT) test pieces. The stress intensity K calibration for this specimen geometry is given by a fourth order polynomial as shown in figure 2. These specimens were machined in the T-L orientation from the center of the plate location. Uniaxial tensile hour glass specimens were also machined in the T-L orientation.

2.3 HEAT TREATMENT

Laboratory heat treatment of the SA542 class 2 steel was performed to produce a variation in material properties. Test

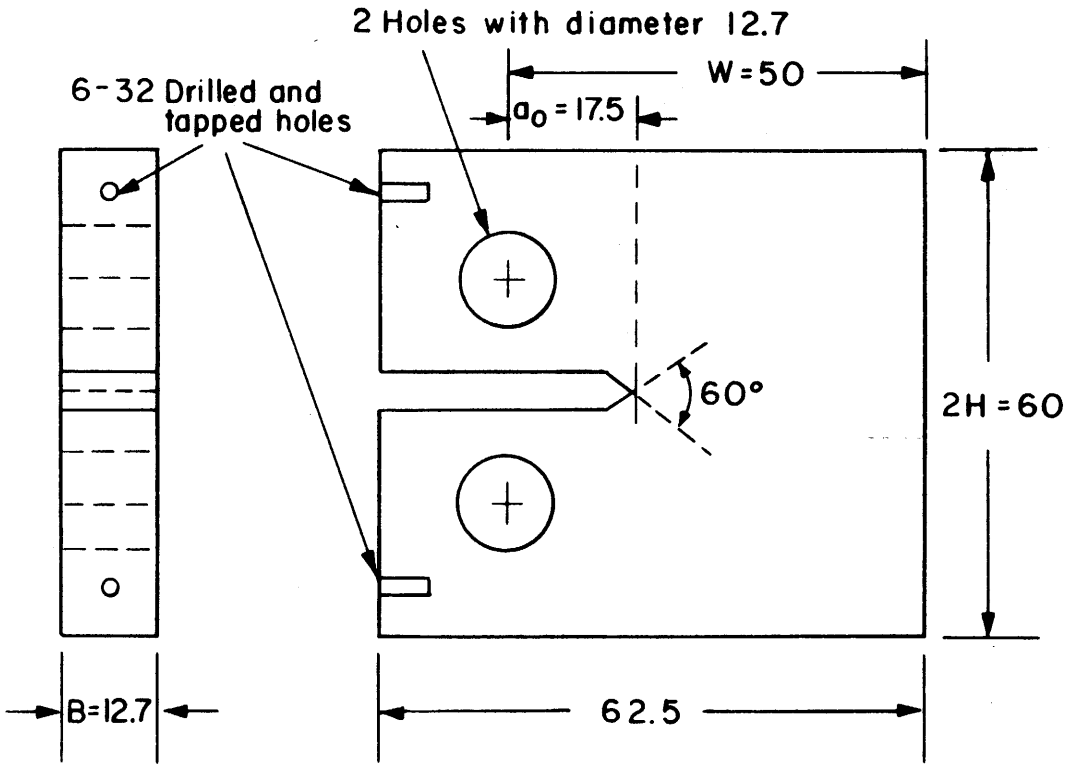

All dimensions in mm

Compact (CT) fatigue testpiece

H/W = 0.60

B = 12.7 mm (0.50 in)

W = 50 mm (1.97 in)

$a_0/W = 0.35$

$$K = \frac{p}{BW^{1/2}} \cdot \frac{(2+\alpha)}{(1-\alpha)^{3/2}} (0.886 + 4.64\alpha - 13.32\alpha^2 + 14.72\alpha^3 - 5.6\alpha^4) \text{ where } \alpha = a/W$$

Fig. 2 Design of compact (CT) testpiece used for fatigue crack propagation tests

pieces were austenitized at 950°C, followed by vigorous water quench. Time specified for austenitizing was 60 minutes per inch of thickness once the specimen outer skin was at furnace temperature. With chromium present in this material, it is important not to exceed the austenitization temperature or time due to chromiums unfavorable promotion of grain growth. Tempering temperatures were 320°C, 470°C, 550°C, 630°C and 690°C. Time of tempering was 90 minutes per inch of specimen thickness and was followed by water quench. A controlled atmosphere furnace was used to treat the machined CT specimens. This furnace, which operated under a vacuum of approximately 10 millitorr, was used to keep decarburization and oxidation to a minimum. Hour glass tensile and metallographic specimens were encapsulated in vycor tubing, then treated in a muzzle furnace. The encapsulating tubes were destroyed upon quenching to permit proper cooling. Rockwell hardness values were taken of all specimens, and compared to previously recorded values to ensure minimal decarburization.

2.4 TEST MACHINES

Fatigue testing was performed on a servo hydraulic 49 kN Instron 1350 testing machine. Experiments were carried out with a sinusoidal tension wave at a frequency of 50 Hz. Environment testing was conducted either in laboratory moist air, or by using a locally mounted environmental chamber system (described in Appendix A) for hydrogen and helium.

2.5 CRACK MONITORING

Fatigue crack length was continuously monitored using the D.C. Electrical Potential technique (16, 17). This method entails passing a constant current (maintained by external means) through a cracked test piece while being loaded (fig. 3). Two 0.010 inch pure iron wire probes are spot welded across the notch and are used to measure the changing specimen resistance during crack growth. By monitoring this resistance and comparing it with the initial potential across the starter notch, the crack length to specimen width (a/W) can be determined with the use of the potential drop. A forty microvolt change in voltage across the crack tip corresponds to a change in crack length of approximately 1mm. The circuit design is based on a system developed by Ritchie (34).

Data reduction involves converting potential-time data to crack length-number of cycles, from which growth rates are obtained through numerical differentiation using finite difference and incremental step polynomial procedures (34). This crack monitoring technique has been shown to measure absolute crack length down to 0.1mm and to detect changes in crack length of the order of 0.01mm.

2.6 TEST PROCEDURE

The threshold stress intensity ΔK_o is computed from the highest stress intensity at which no growth can be detected within 10^7 cycles. Therefore using this crack monitoring technique, the

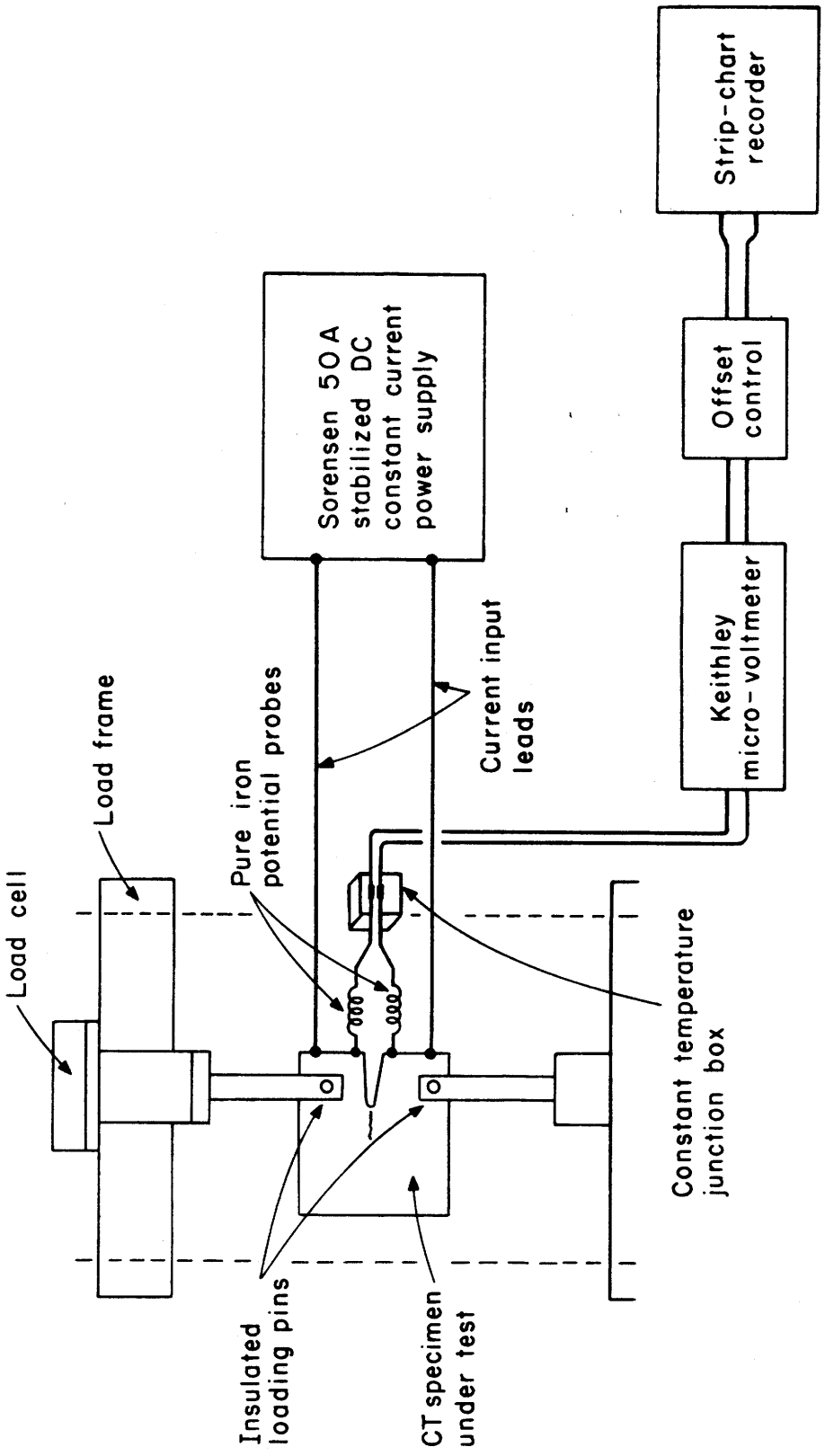

Fig. 3 Schematic diagram of electrical potential crack monitoring system.

threshold ΔK_0 can be defined in terms of a maximum growth rate of 10^{-8} mm/cycle (4×10^{-10} in/cycle). The value of the threshold ΔK_0 is found using a load shedding technique (fig. 4). This technique initiates a fatigue crack from the specimen notch at a ΔK corresponding to the mid growth regime, at a relatively high growth rate. Once the crack has initiated, the loads are then successively decreased by not more than 10% of the previous load. This is to prevent any premature crack arrest due to residual plastic deformation. The crack is grown, for each load, a distance of at least four times the maximum plastic zone size[1] from the previous load. This is to minimize transient crack growth effects from residual plasticity. Once the loads have been decreased to the threshold ΔK_0 (5 - 6 days), the mid growth data are obtained using a constant load (increasing ΔK).

2.7 FRACTOGRAPHY

Fracture surfaces were analyzed using a scanning electron microscope (SEM). Fractographs were taken at a range of ΔK values for each fatigue test performed. In each case, the fracture mechanism is noted and correlated to stress intensity, load ratio, environment and material strength. The proportion of intergranular fracture (facets), as a function of ΔK, was measured using a grid method. A transparent grid of 100 squares per inch

---

[1] maximum plastic zone size $r_\gamma \cong \frac{1}{2\pi} \left(\frac{K_{max}}{\sigma_\gamma}\right)^2$

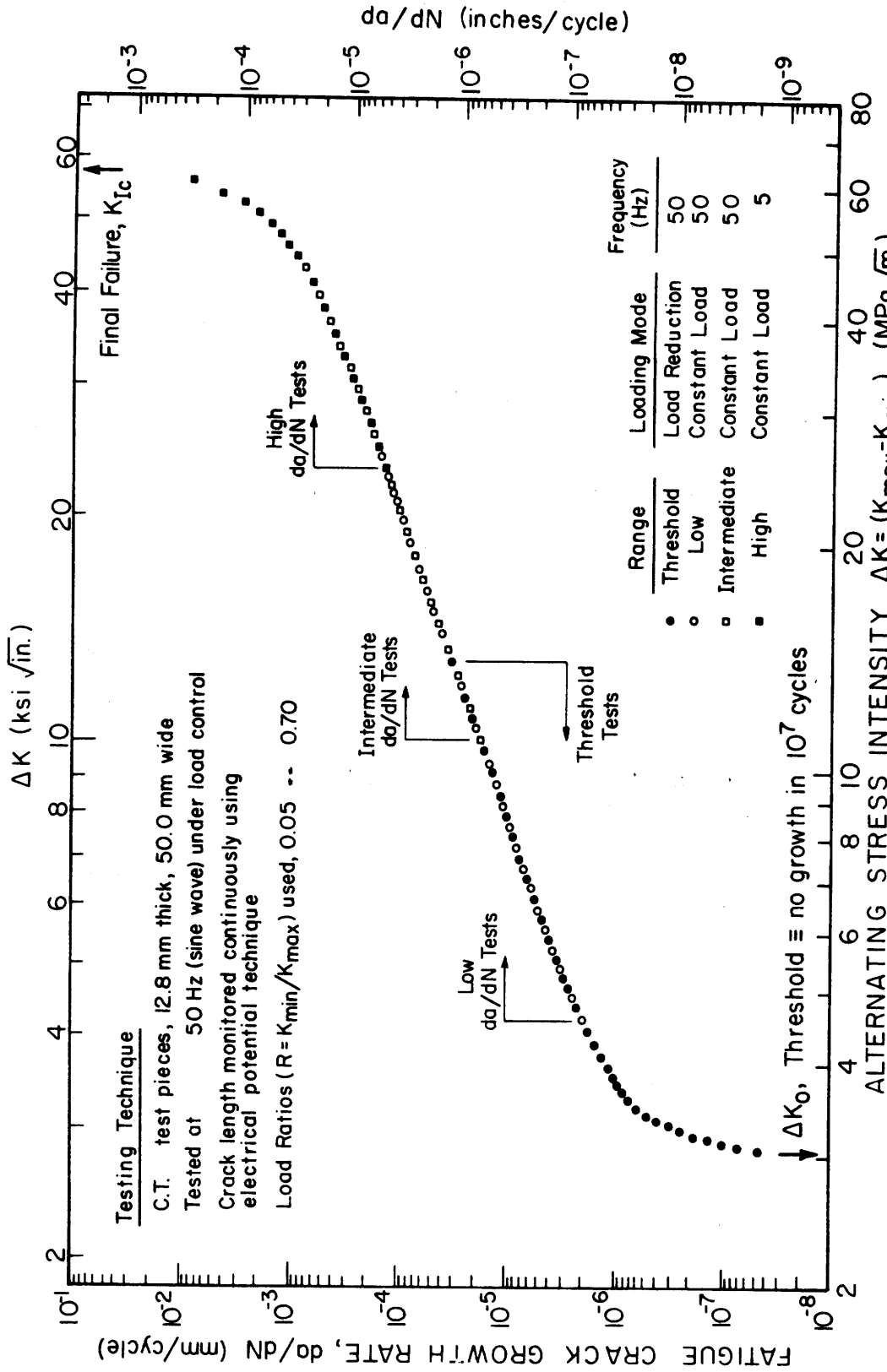

Fig. 4: Typical test procedures for obtaining fatigue crack propagation data spanning the entire range of growth rates from threshold levels to final fatigue.

was placed over the fractograph. The percentage of intergranular fracture was then calculated by an area fraction.

CHAPTER III

RESULTS

3.1 MATERIAL PROPERTIES AND MICROSTRUCTURAL ANALYSIS

The resulting variation of uniaxial tensile properties with tempering temperature is shown in figure 5. This plot indicates a trend of decreasing material strength and increasing ductility with increasing tempering temperature. The only exception to this trend occurs at approximately 500°C - 600°C, where the effect of secondary hardening is seen. The presence of chromium and molybdenum form part of the carbide phase and thus bring about this retardation of softening. The rapid decrease in material strength with increasing tempering temperature above the secondary hardening peak is typical for 2 1/4 Cr - 1 Mo steel (39), and demonstrates the need for close temperature control when tempering this material.

The yield strength values varied from a low of 575 MPa (83ksi) at the 690°C temper to a maximum of 951 MPa (138 ksi) at the 320°C temper (Table I). The as-received condition (638°C temper) produced a mid value of 769 MPa (111 ksi).

Figure 6 shows optical micrographs of the SA542 class 2 steel in the as-received, 320°C, 630°C and 690°C temper conditions. These micrographs indicate a fully transformed, acicular tempered martensitic structure with no evidence of pro-eutectoid ferrite. This is in contrast to commercially

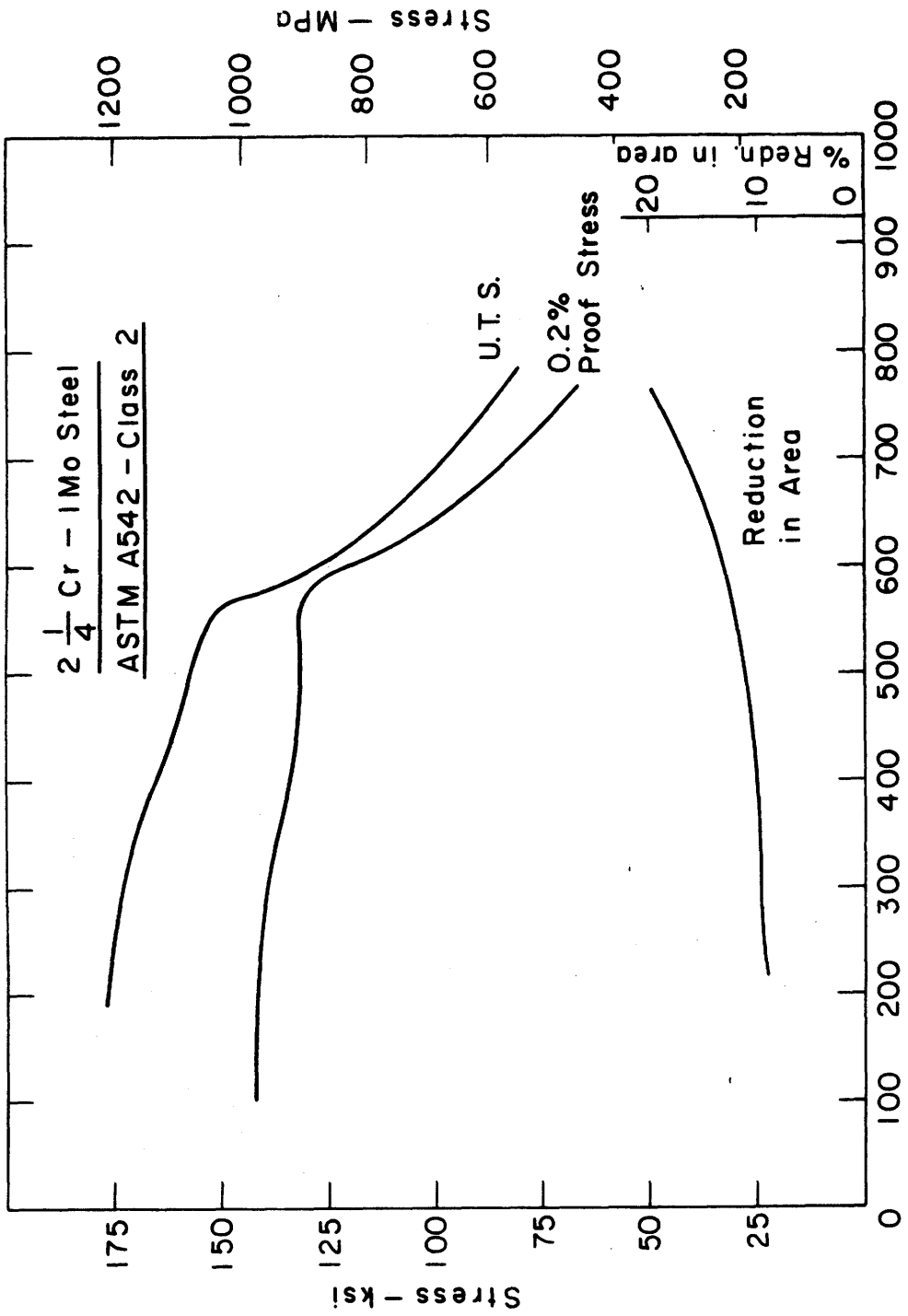

Fig. 5 Effect of tempering temperature on ambient temperature uniaxial tensile properties of SA542 Class 2 steel, water quenched from 950°C

Heat Treatment	Microstructure[3]	Grain size (μm)	0.2% Proof Stress (MPa)	U.T.S. (MPa)	Elongation[1] (%)	Red. in Area (%)	Hardness (R_B)
As-received	100% M[2]	40	761	838	15.8	70.5	83
Tempered at 320°C	100% M + ε carbide	40	951	1186	10.2	47.3	102
Tempered at 470°C	100% M + ε carbide	40	917	1096	10.7	51.8	103
Tempered at 550°C	100% M + Fe_3C + Mo_2C	40	917	1058	11.1	53.1	103
Tempered at 630°C	100% M + Fe_3C + Mo_2C	40	717	800	14.1	60.2	92
Tempered at 690°C	100% M + Fe_3C + Mo_2C	40	575	679	17.0	65.2	90

[1]For 33 mm gauge length

[2]Martensite

[3]Reference (37)

Table 1: Table of property variation due to laboratory heat treatment which includes tempering at 320°C, 470°C, 550°C, 630°C and 690°C.

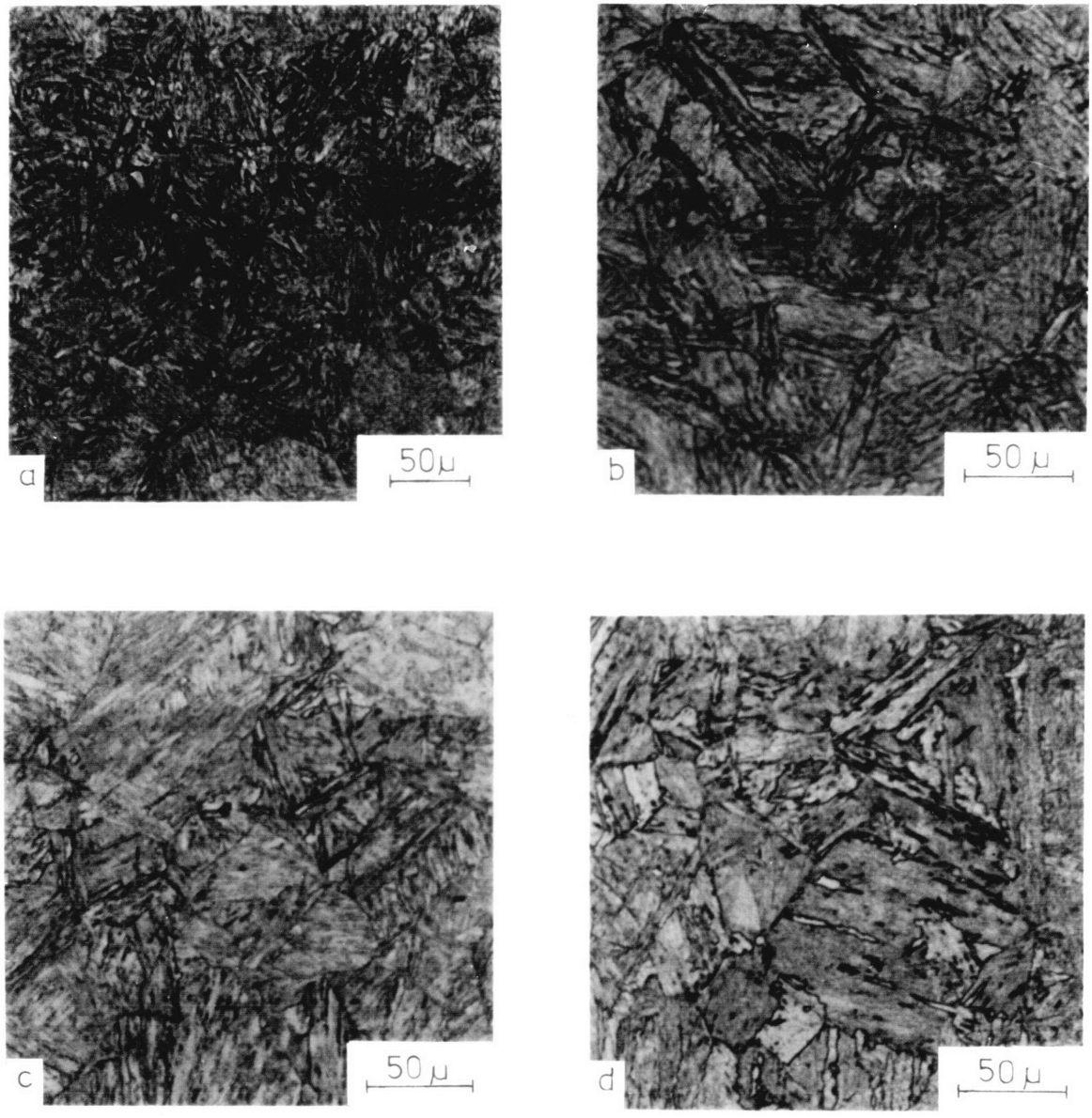

Fig. 6 Optical micrographs of SA542 class 2 (25 mm thick) plate austenitized at 950°C, water quenched and tempered: (a) as-received (b) 320°C temper (c) 630°C temper and (d) 690°C temper.

quenched and tempered SA542 thick plate material which is predominantly bainitic (1). Differences in the microstructures with increasing tempering temperature cannot be resolved with optical microscopy (1). However, for tempering times used, it is probable that autotempered ε-carbides present in the as-quenched structure are replaced by cementite around 550°C with additional precipitation of Mo_2C and spheroidization of Fe_3C occurring above 650°C (37).

3.2 INFLUENCE OF MATERIAL STRENGTH ON NEAR-THRESHOLD GROWTH RATES

Near-threshold fatigue crack growth tests were performed on SA542 class 2 steel over a range of material yield strengthes: 575 MPa (690°C temper), 769 MPa (as-received) and 951 MPa (320°C temper). It is important to point out that the variation in material strength was produced with no change in prior austenite grain size. All material strength tests were performed in moist air at a load ratio of R = 0.05. Figure 7 is a plot of crack growth data for the 575 MPa and 769 MPa conditions. The threshold ΔK_o was lowered by 17% from a value of 8.6 MPa $\sqrt{m}$ for the 575 MPa strength to 7.1 MPa $\sqrt{m}$ for the 769 MPa strength condition. The corresponding near-threshold crack growth rates were increased by up to 100 times, with this increase in yield strength. Test conducted on the 320°C temper condition produced questionable results, possibly due to residual stresses present. Therefore the 320°C temper results and problems are described in Appendix B.

Several investigators have shown this effect of increasing near-threshold growth rates with increasing mechanical strength. Ritchie (5) reported such a trend in ultra-high strength (yield stress = 1000-1800 MPa) 300M steel at R = 0.05. Work by Moss(6) on normalized 2 1/4 Cr - 1 Mo (SA387-2-22) low strength steel displayed a decrease in threshold ΔK_o of 10% upon increasing yield strength from 290 MPa to 390 MPa. These tests were performed in moist air at a load ratio of 0.05. Suresh (53)

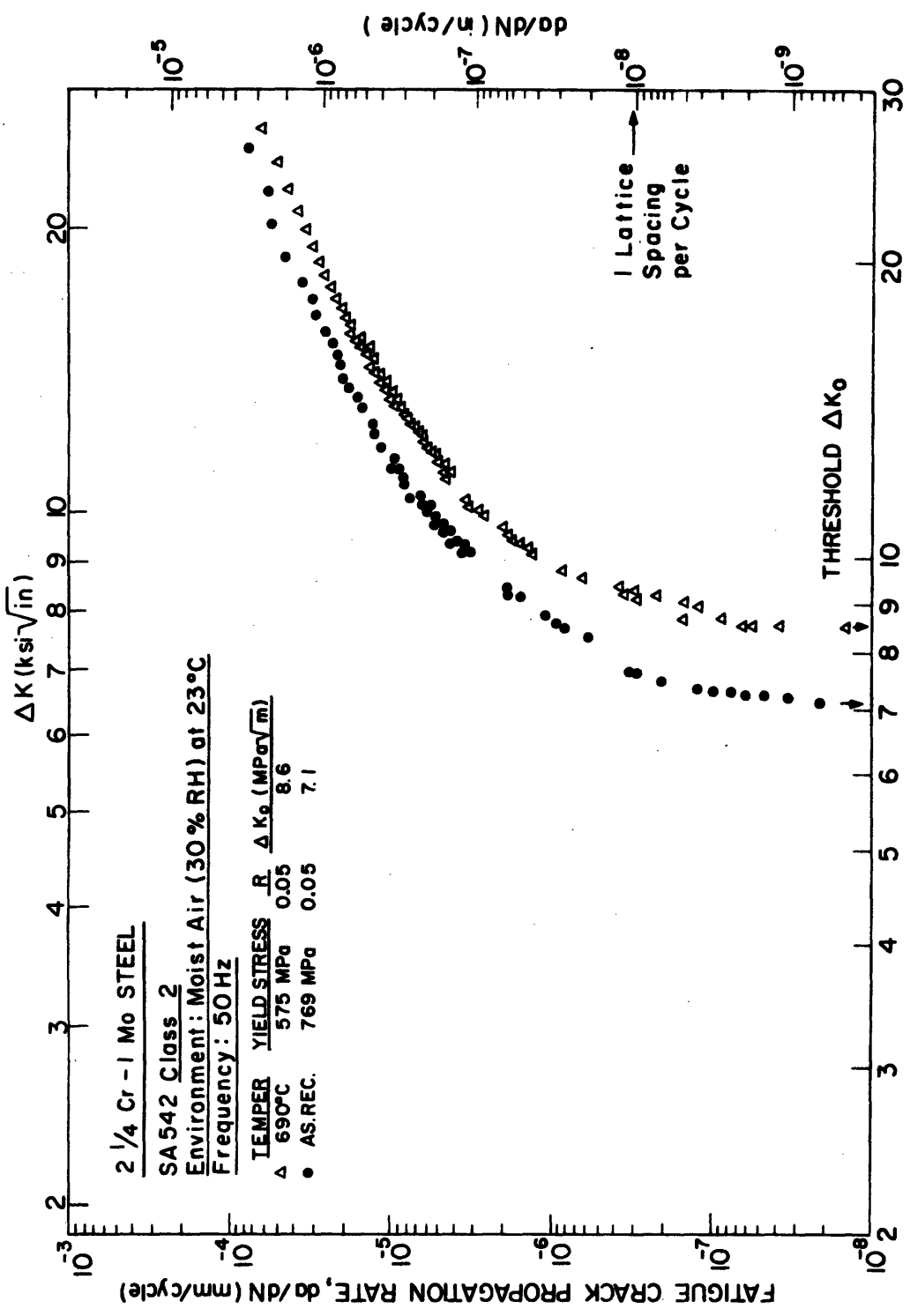

Fig 7: Effect of yield strength on fatigue crack propagation in SA542 steel tested in moist air.

tested the thick section, quenched and tempered SA542 class 3 steel of fully bainitic microstructure. These tests showed a decrease in threshold ΔK_0 from 7.7 MPa $\sqrt{m}$ for the center thickness location (485 MPa) to 7.4 MPa $\sqrt{m}$ for the surface material (500 MPa). Figure 8 is a plot of threshold ΔK_0 values versus material yield strength taken for a number of steel conditions. The general trend is a decrease in threshold ΔK_0 with increasing strength. Data on 2 1/4 Cr - 1 Mo steels from work by Moss (6) and Suresh (53) were plotted along with the threshold ΔK_0 for SA542 class 2 steel in the as-received condition. These points are connected, and are seen to follow the general trend. An important factor in the dependency of near-threshold growth on material strength is microstructure (grain size, phase, etc.). As a general rule, martensitic steels tend to offer the least resistance to near-threshold growth. Bainitic steels display a higher resistance and ferritic/pearlitic steels exhibit the most resistance, of these structures, to near-threshold growth.

As a generality, fatigue crack growth is insensitive to material strength except in the near-threshold regime. In the mid growth regime, raising the strength of steels by nearly an order of magnitude does not change growth rates by more than a factor of 2 or 3 (25). This similarity in growth rates above 10^{-6} mm/cycle is consistent with the fact that the mid growth regime is often independent of microstructure. To summarize,

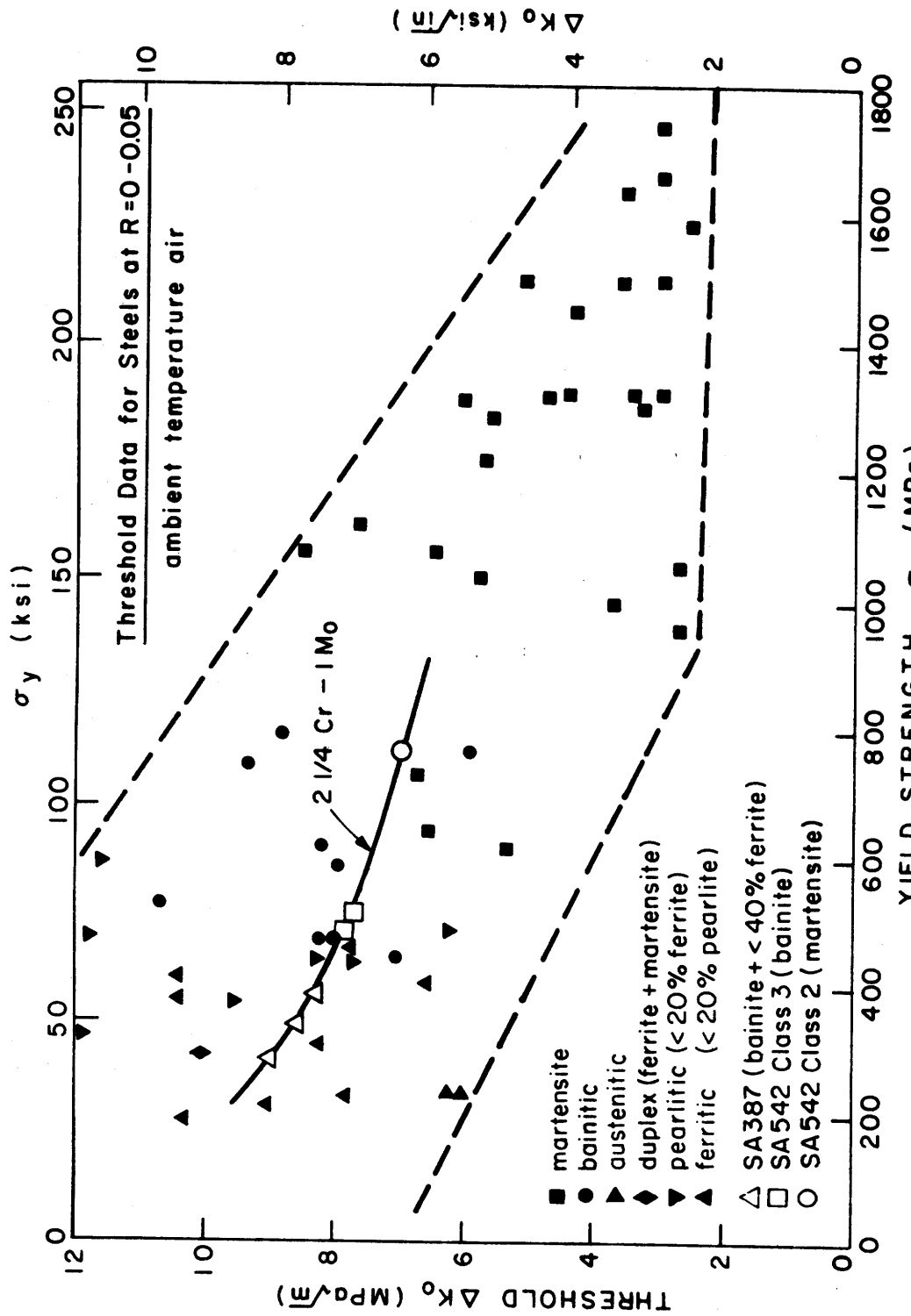

Fig. 8. Variation of threshold ΔK_o (at R = 0 - 0.05) with yield strength for steels (σ_y = 200 - 1800 MPa).

this phase of the study showed a decrease in threshold ΔK_o and an increase in near-threshold growth rates with a change in yield strength from 575 MPa to 769 MPa.

Future testing on this material is needed to provide threshold ΔK_o values for the range of tempering temperatures that may have applicability in service.

3.3 INFLUENCE OF LOAD RATIO ON NEAR-THRESHOLD GROWTH RATES

One of the most striking characteristics of near-threshold growth is a marked dependency on mean stress, characterized by load ratio ($R = {}^{K_{min}}/_{K_{max}}$). This is particularly relevant to service conditions where high mean stresses are present from applied operating stresses (pressure vessels) and residual stresses. Many authors (5-7, 9-11, 13, 20, 22, 23, 46, 48) have shown for a wide range of steels and non-ferrous alloys that high load ratios markedly decrease near-threshold crack growth resistance.

To determine the influence of load ratio on the quenched and tempered fully martensitic SA542 class 2 steel, tests were performed on the as-received material condition at load ratios of 0.05 and 0.75. Figure 9 displays the very significant decrease in threshold ΔK_o for tests in moist air from 7.1 MPa $\sqrt{m}$ for R = 0.05 to 2.8 MPa $\sqrt{m}$ for R = 0.75. This corresponds to a 60% decrease in threshold ΔK_o. The corresponding near-threshold growth rates were increased by up to <u>three</u> orders of magnitude. It is clearly seen that for alternating stress intensities (ΔK) between 3.0 MPa $\sqrt{m}$ and 7.0 MPa $\sqrt{m}$ there will be no detectable growth for a load ratio of 0.05, whereas growth will be at a relatively high rate (10^{-7} mm/cycle to 10^{-5} mm/cycle) for a load ratio of 0.75. Moss (6) reported similiar results with a decrease in threshold ΔK_o of 40% for tests on a lower strength normalized 2 1/4 Cr - 1 Mo steel in moist air at load ratios

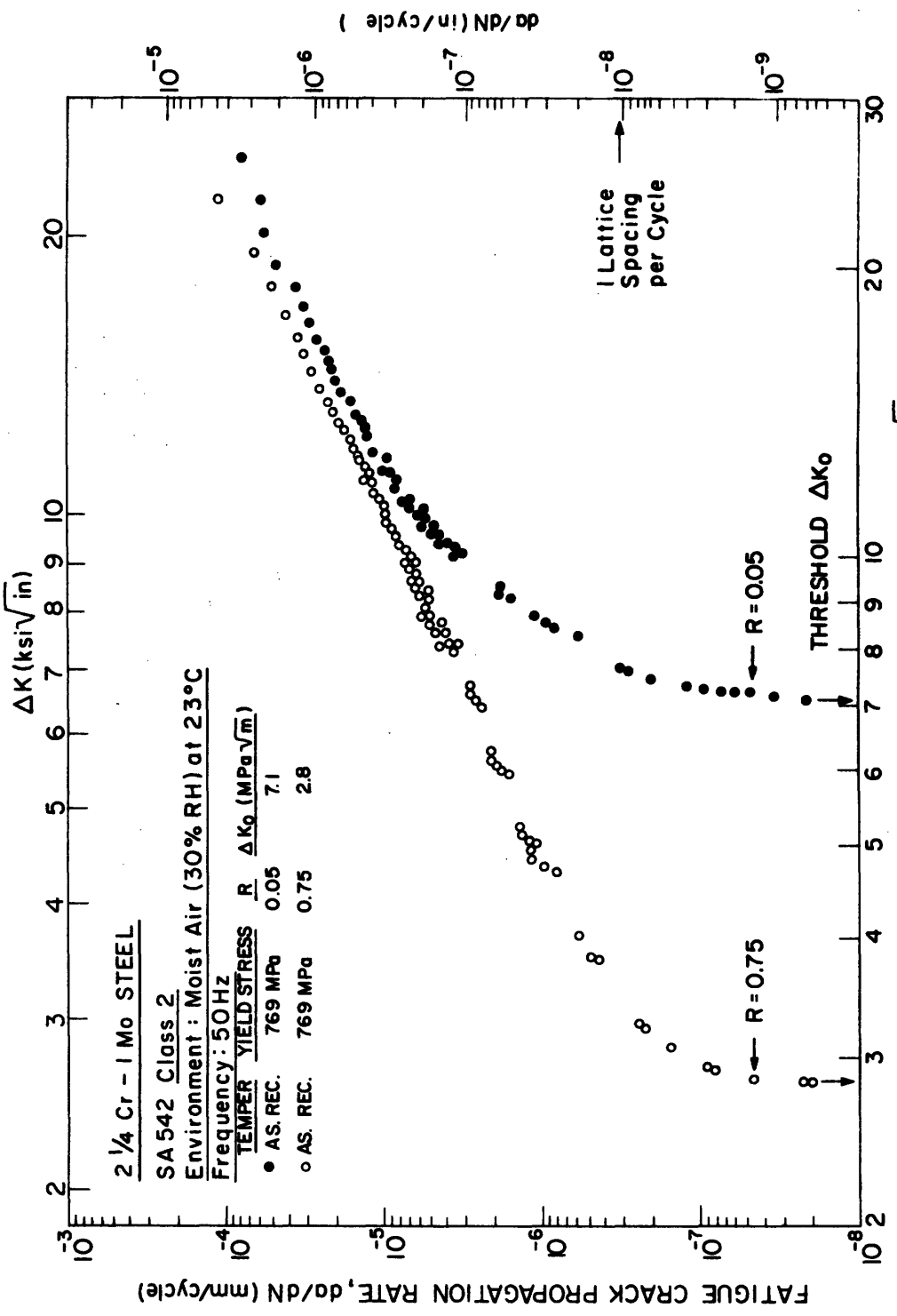

Fig. 9. Effect of load ratio on near-threshold fatigue crack propagation for the as-received material tested in moist air.

of 0.05 and 0.80.

Load ratio tests in UHP helium and UHP hydrogen displayed the same effect of decreasing threshold ΔK_0 with increasing R. Figure 10, for tests in helium, exhibits a decrease in threshold ΔK_0 from 4.9 MPa $\sqrt{m}$ to 2.7 MPa $\sqrt{m}$, upon increasing the load ratio from 0.05 to 0.75. This effect on near-threshold growth is in contrast to tests in inert (vacuum) environments by Beevers and co-workers (30, 46) on tempered martensitic En 24 steel, and Irving and Kurzfield (76), where threshold ΔK_0 was found to be independent of load ratio. Therefore, the results in helium tend to indicate a problem of what is an inert environment. Clearly, the vacuum and inert gas environments are very different as far as the effect on near-threshold growth.

Tests in hydrogen (fig. 11) showed a similar change in ΔK_0 from 4.6 MPa $\sqrt{m}$ to 2.8 MPa $\sqrt{m}$. Figure 12 is a plot of threshold ΔK_0 values versus load ratio for the three test environments. It can be seen that each case displays a trend of decreasing threshold ΔK_0 with increasing load ratio R. It is also clear that tests in moist air produced the largest change in threshold values. A model that is qualitatively consistent with these results is given in the discussion chapter.

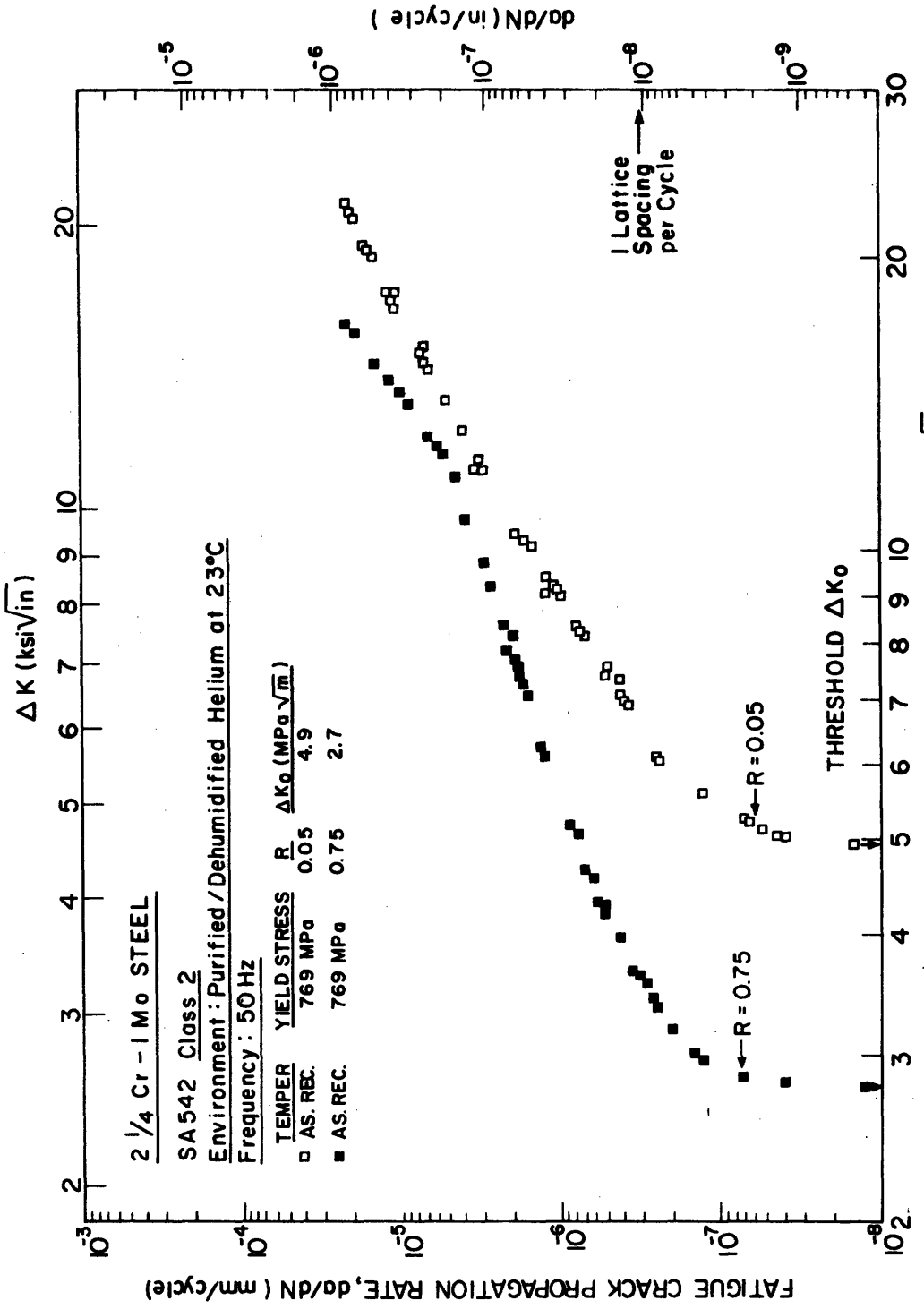

Fig. 10: Effect of load ratio on near-threshold fatigue crack propagation for the as-received material tested in UHP helium.

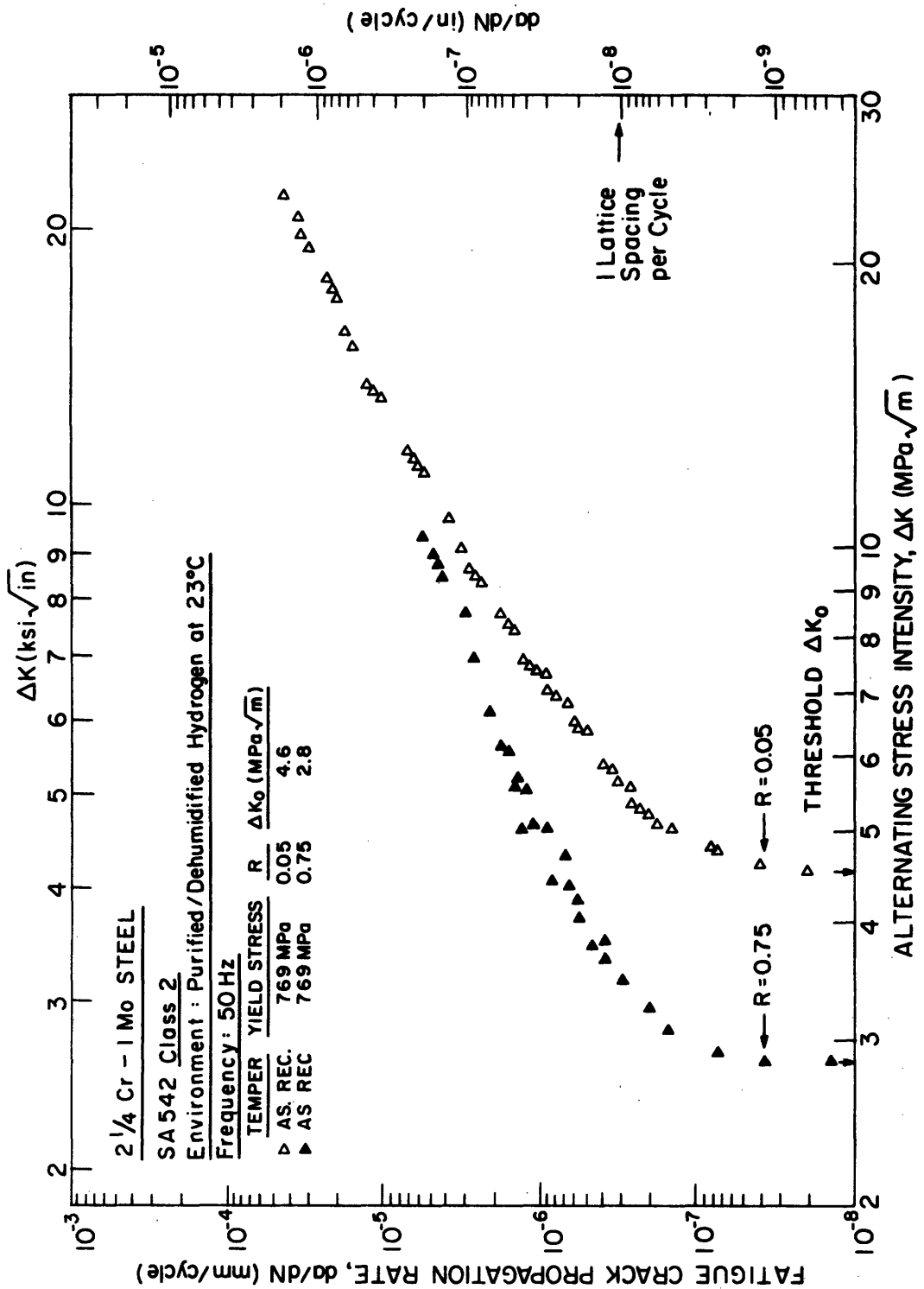

Fig. 11: Effect of load ratio on near-threshold fatigue crack propagation for the as-received material tested in UHP hydrogen.

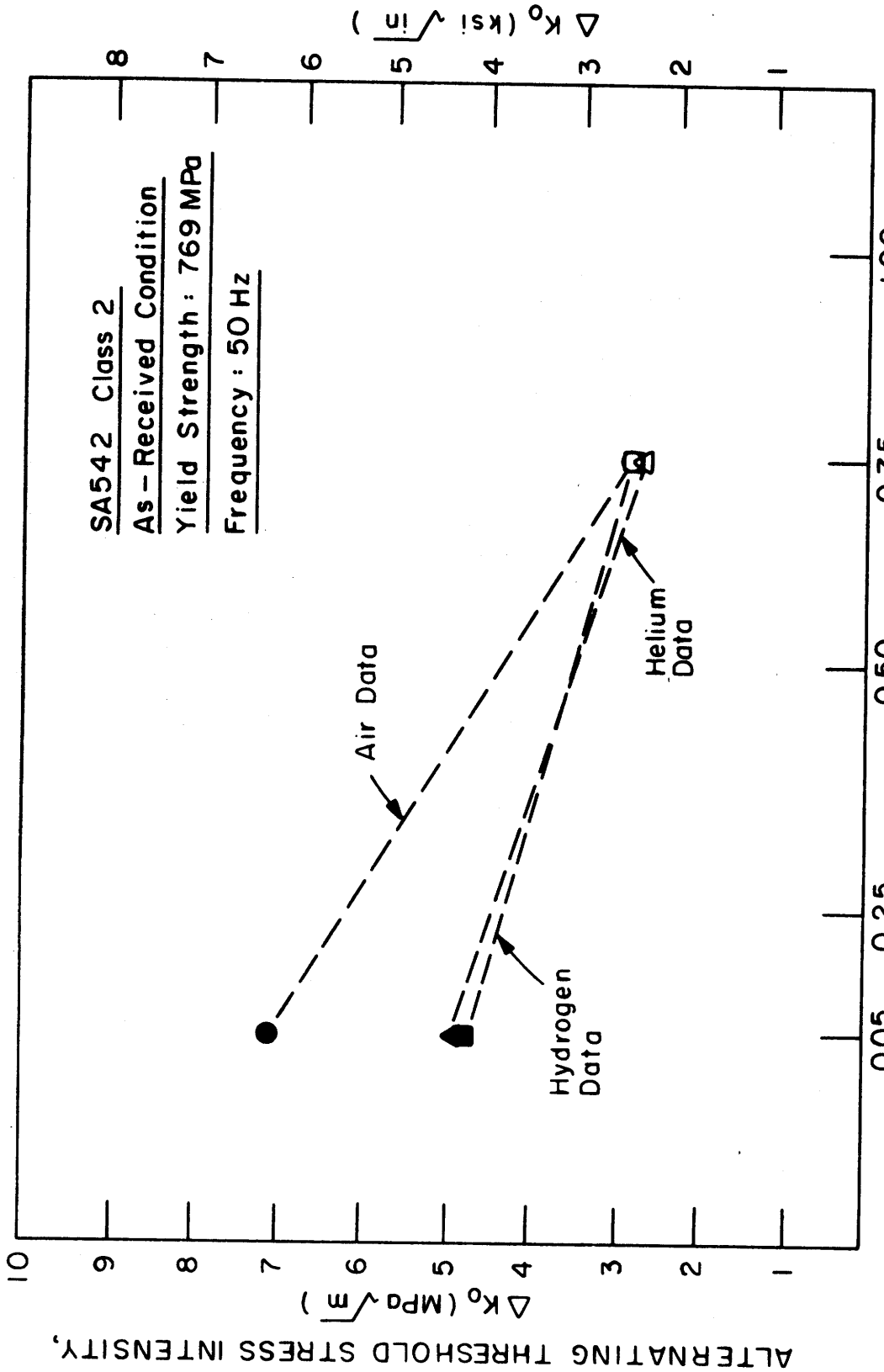

Fig. 12: Variation of alternating threshold stress intensity ΔK_o with load ratio for SA542 class 2 in air, hydrogen and helium.

3.4 INFLUENCE OF ENVIRONMENT ON NEAR-THRESHOLD GROWTH RATES

Tests were conducted on the quenched and tempered fully martensitic SA542 class 2 steel to determine the influence of environment on near-threshold behavior. The test environments consisted of moist air (30% relative humidity), UPH hydrogen and UHP helium. Figure 13 is a plot of growth rate versus ΔK for the as-received material tested in moist air and UHP hydrogen,as a function of load ratio. At low R, the threshold ΔK_o is significantly reduced from 7.1 MPa $\sqrt{m}$ for moist air to 4.6 MPa $\sqrt{m}$ for hydrogen. This corresponds to a 35% decrease in ΔK_o, while the near-threshold growth rates increased by up to two orders of magnitude. Tests at high R showed no influence of hydrogen on near-threshold growth rates or on ΔK_o, compared to moist air. Both tests displayed similar growth rates, and identical ΔK_o values of 2.8 MPa $\sqrt{m}$. The mid growth regime was relatively independent of environment and load ratio for this set of tests. Figure 14 is a plot of growth rates for the as-received material tested in UHP helium and moist air. At low R, the threshold ΔK_o was decreased from 7.1 MPa $\sqrt{m}$ for moist air to 4.9 MPa $\sqrt{m}$ for the purified helium environment. The near-threshold growth was again independent of environment at high load ratio. The mid growth regime did display lower growth rates for the helium tests compared to air and hydrogen for both load ratios. This observation of lower mid growth rates for the inert environment may tend to

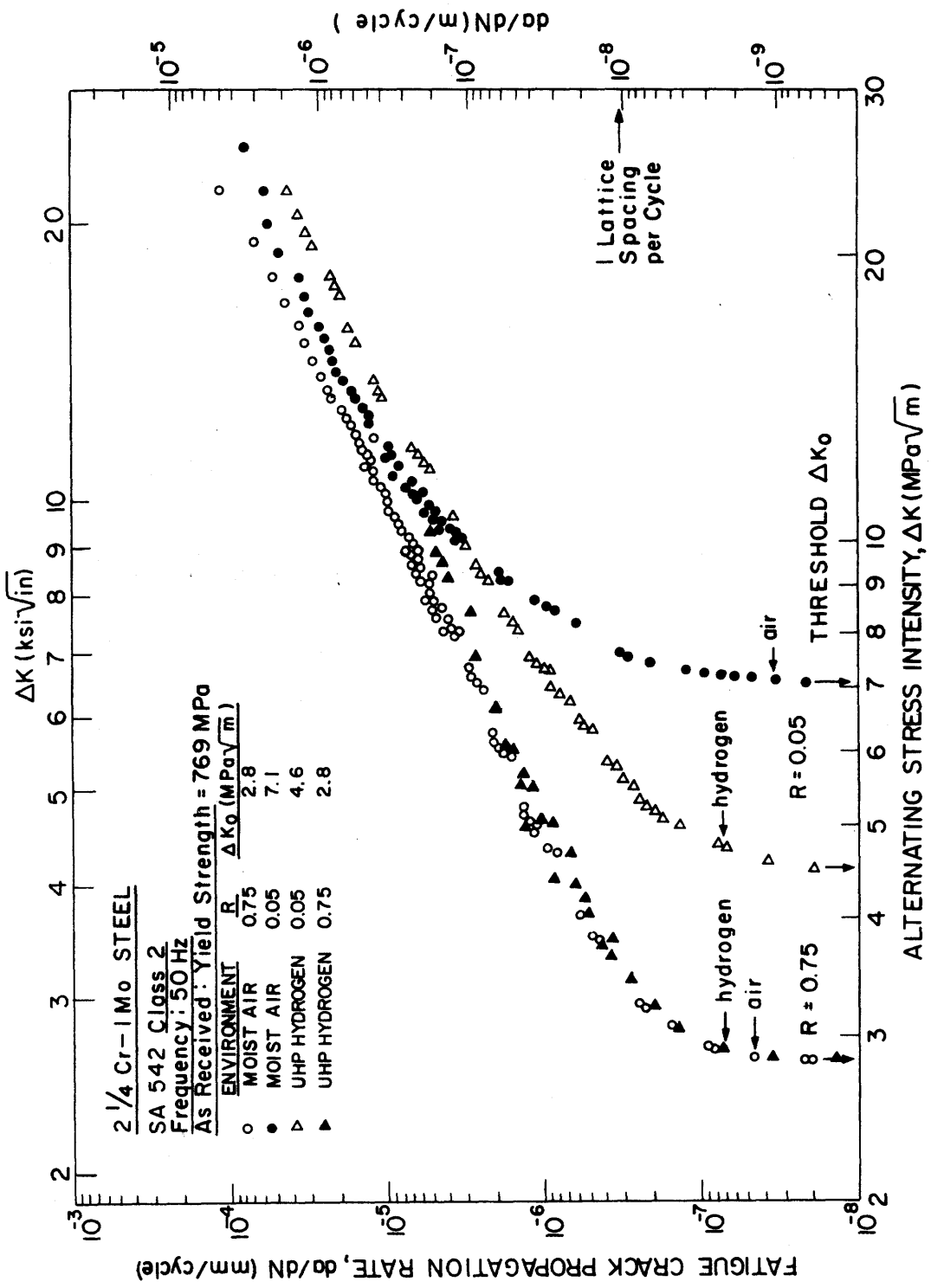

Fig. 13: Variation in near-threshold fatigue crack propagation with load ratio for the as-received material condition in air and hydrogen.

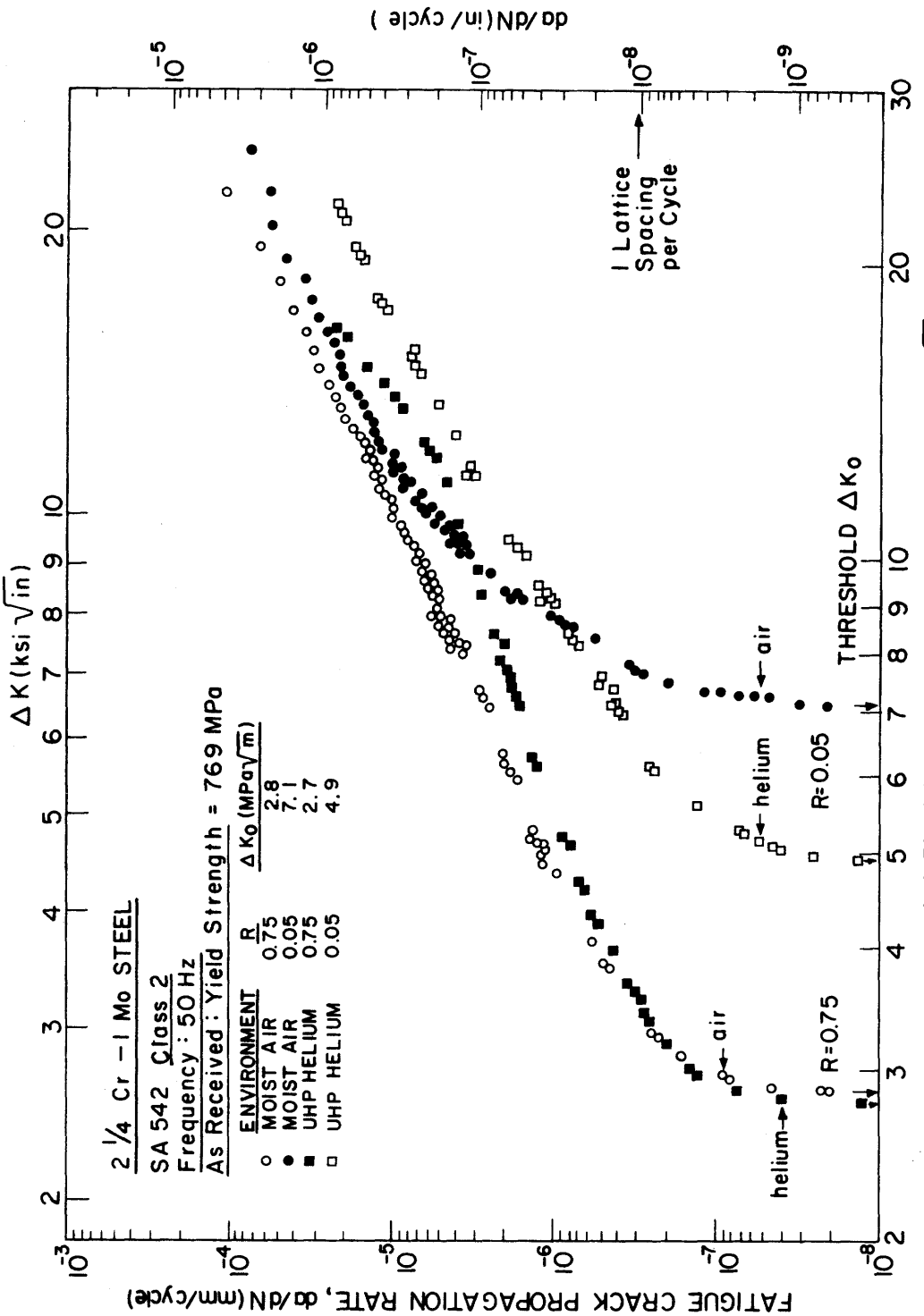

Fig. 14. Variation in near-threshold fatigue crack propagation with load ratio for the as-received material condition in air and helium.

indicate that there is some form of environmental growth enhancement for this regime.

The helium/air trend of threshold ΔK_o change with environment is almost identical to that of the previous hydrogen/air data (fig. 15). This is somewhat surprising since the intiative to test in a purified inert environment was to remove or isolate any environmental effect. Similar results were found for tests on the 690°C temper condition. Figure 16 is a plot of growth rates at a load ratio of 0.05 for moist air, UHP hydrogen and UHP helium. The main point to be stressed from these data is the enhanced near-threshold growth for hydrogen and helium compared to moist air, and how the mid growth regime again shows slower growth for the inert helium environment. Figures 17 and 18 are comparisons of the as-received and 690°C temper condition at low R for air/hydrogen and air/helium. These plots are intended to show the trend observed in these tests whereby hydrogen is seen to enhance near-threshold growth compared to moist air, and that helium produces a similar effect. Also, that the mid growth regime displays lower growth rates for the inert environment.

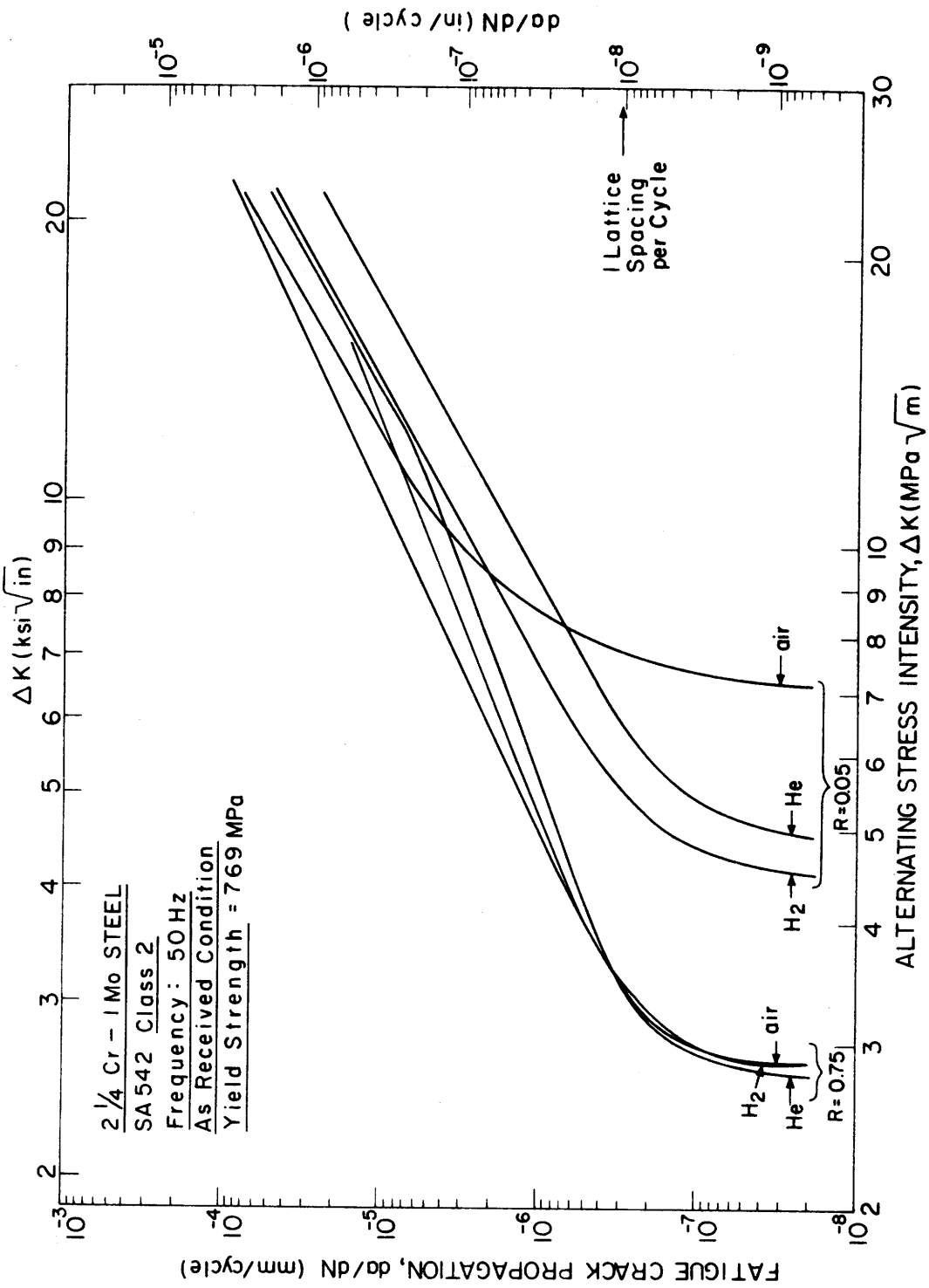

Fig. 15: Schematic plot of variation in near-threshold fatigue crack propagation with environment and load ratio for the as-received material condition.

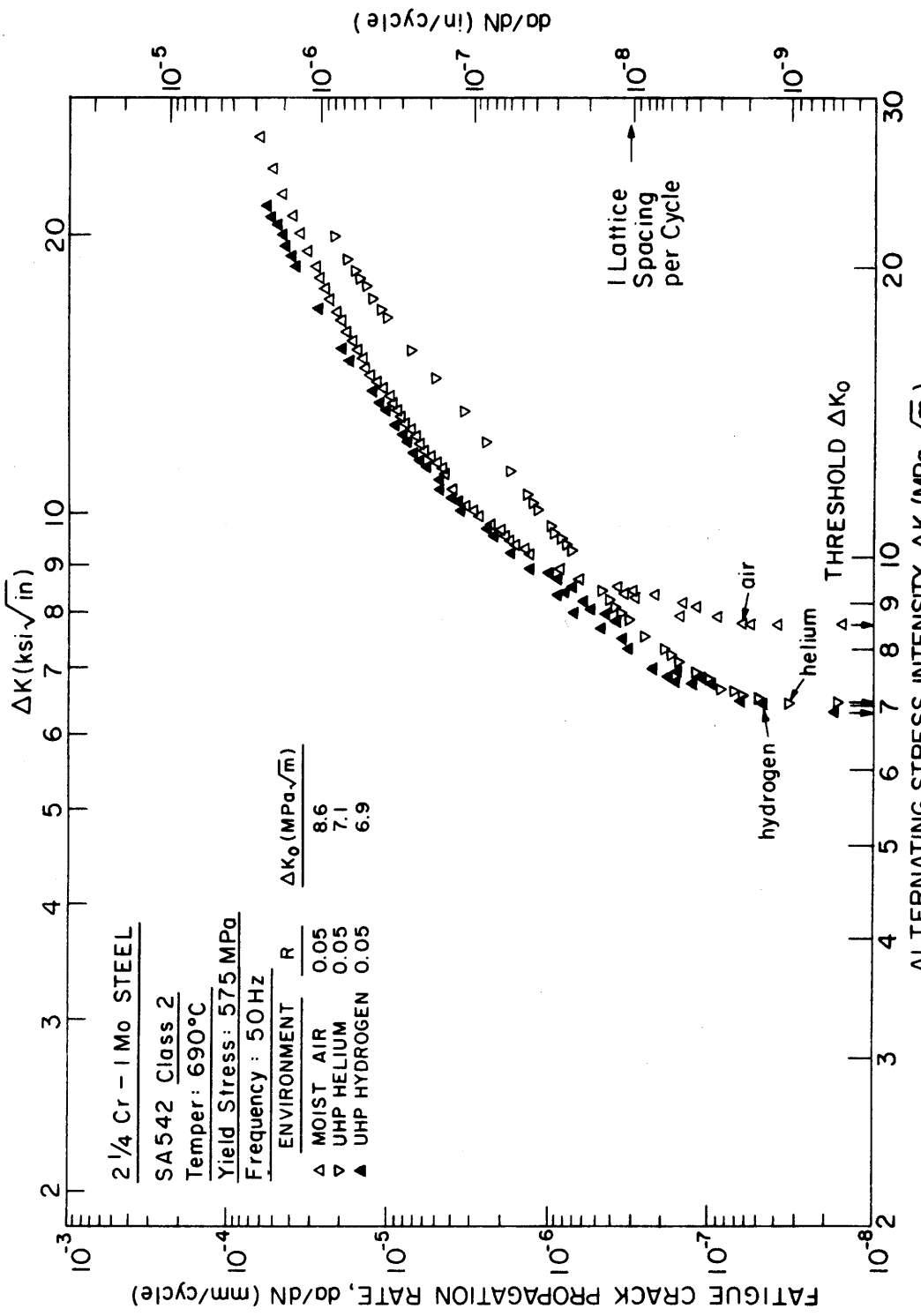

Fig. 16: Variation in near-threshold fatigue crack growth for 690°C temper condition in air, hydrogen and helium at R = 0.05.

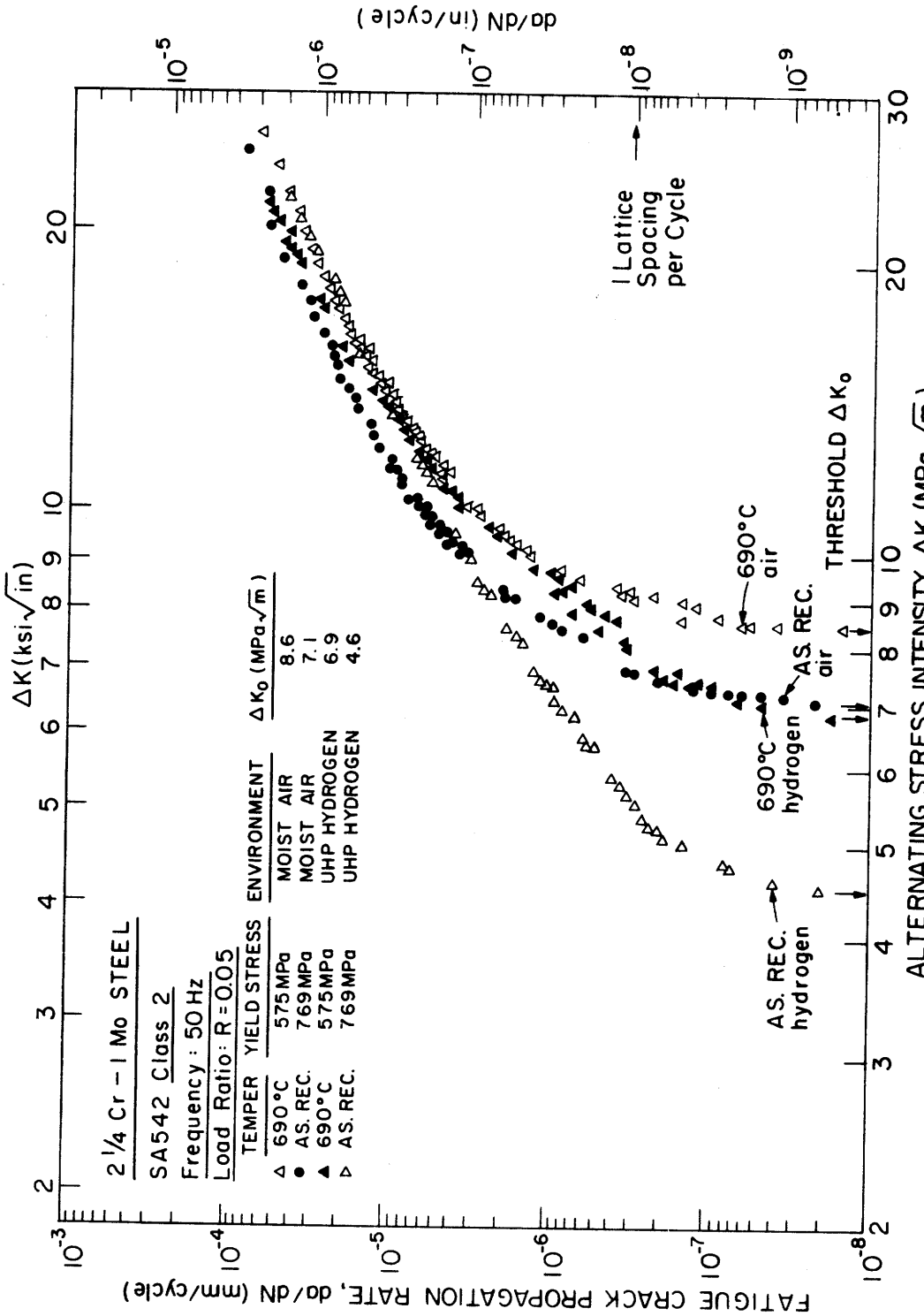

Fig. 17: Comparison of near-threshold fatigue crack growth between the as-received and 690°C temper material in moist air and hydrogen at R = 0.05.

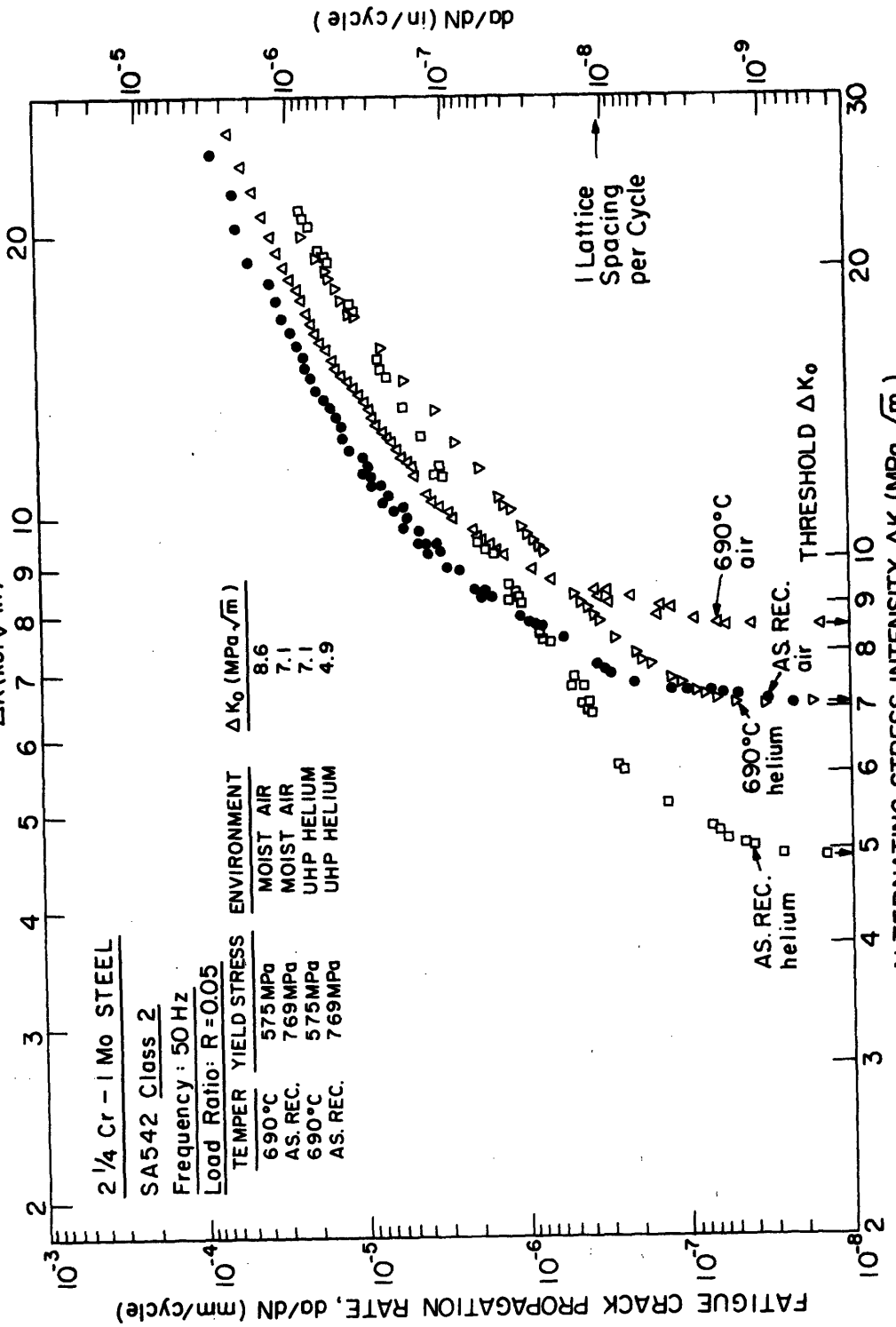

Fig. 18: Comparison of near-threshold fatigue crack growth between the as-received and 690°C temper material in moist air and helium at R = 0.05.

3.5 FRACTOGRAPHY

The fracture surfaces of the fatigue cracks produced in the various environments were examined using a scanning electron miscroscope. It was found that the fracture modes were dependent on the alternating stress intensity, load ratio and environment. At near-threshold levels crack growth is characterized by a predominantly fine scale transgranular mechanism, which is typical of near-threshold fatigue surfaces in a wide range of steels (5, 7, 29, 30), with varying percentages of intergranular (IG) facets.

Fractographs displaying the fracture surfaces for the as-received material near the threshold ΔK_0 for both low and high R are shown on figure 19 as a function of environment. At low R (0.05), all three environments (a, c, e) showed a transgranular fracture, with only the air and hydrogen displaying any IG fracture (less than 3%). At high R (0.75), the hydrogen and helium fracture surfaces exhibited a finer scale transgranular mode than the air test, with no IG fracture observed.

The fracture surfaces for the as-received material at low R are shown in figure 20 as a function of ΔK and environment. Figure 21 is a plot of intergranular fracture versus ΔK as a function of environment. The air tests display a maximum of 46% IG fracture at a ΔK of 14 MPa $\sqrt{m}$, whereas hydrogen shows a peak at 31% (ΔK = 14 MPa $\sqrt{m}$) and helium at 14%

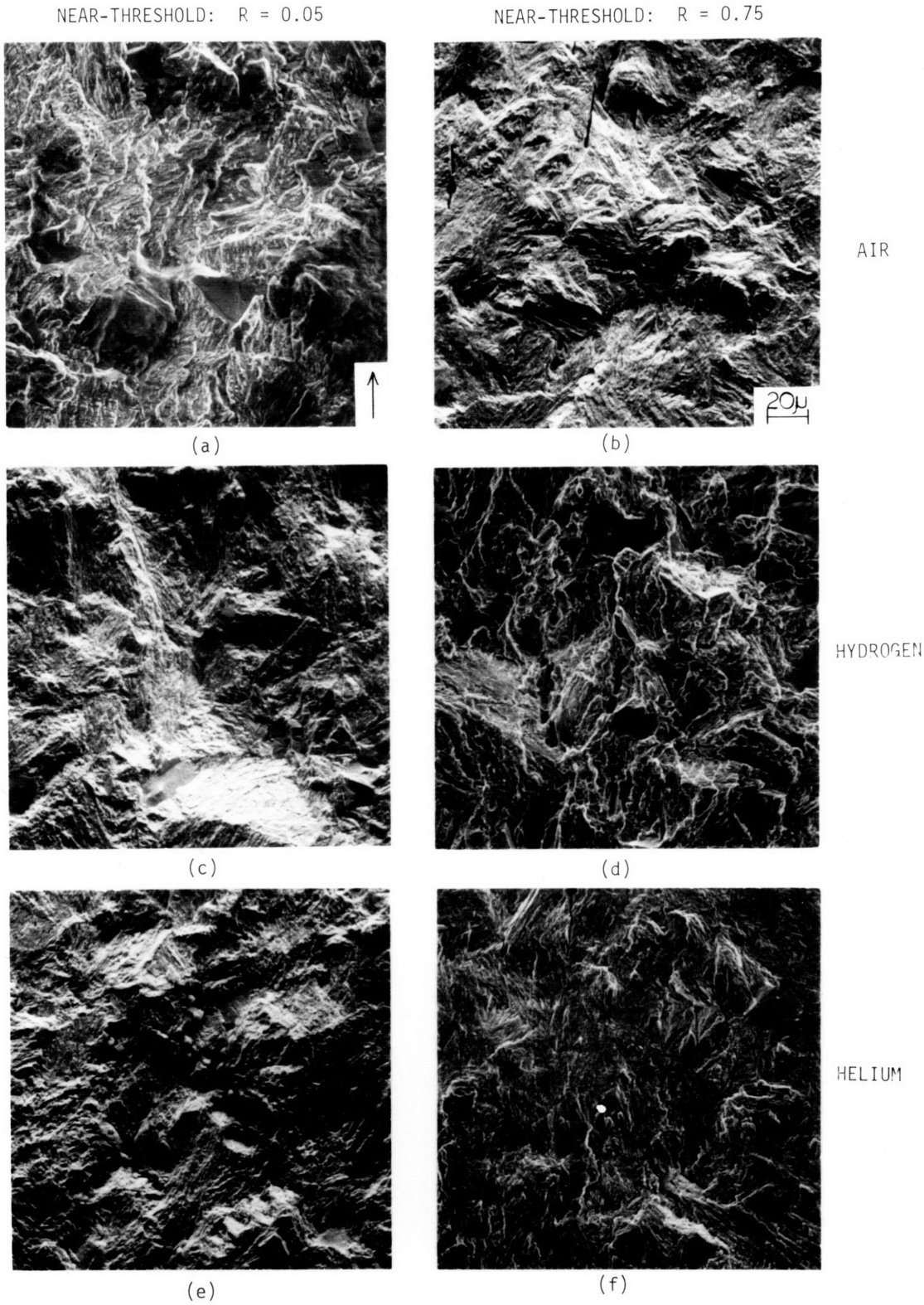

Fig. 19 Comparison of fracture surfaces in air, hydrogen and helium near the threshold ΔK for the as-received condition as a function of the load ratio.

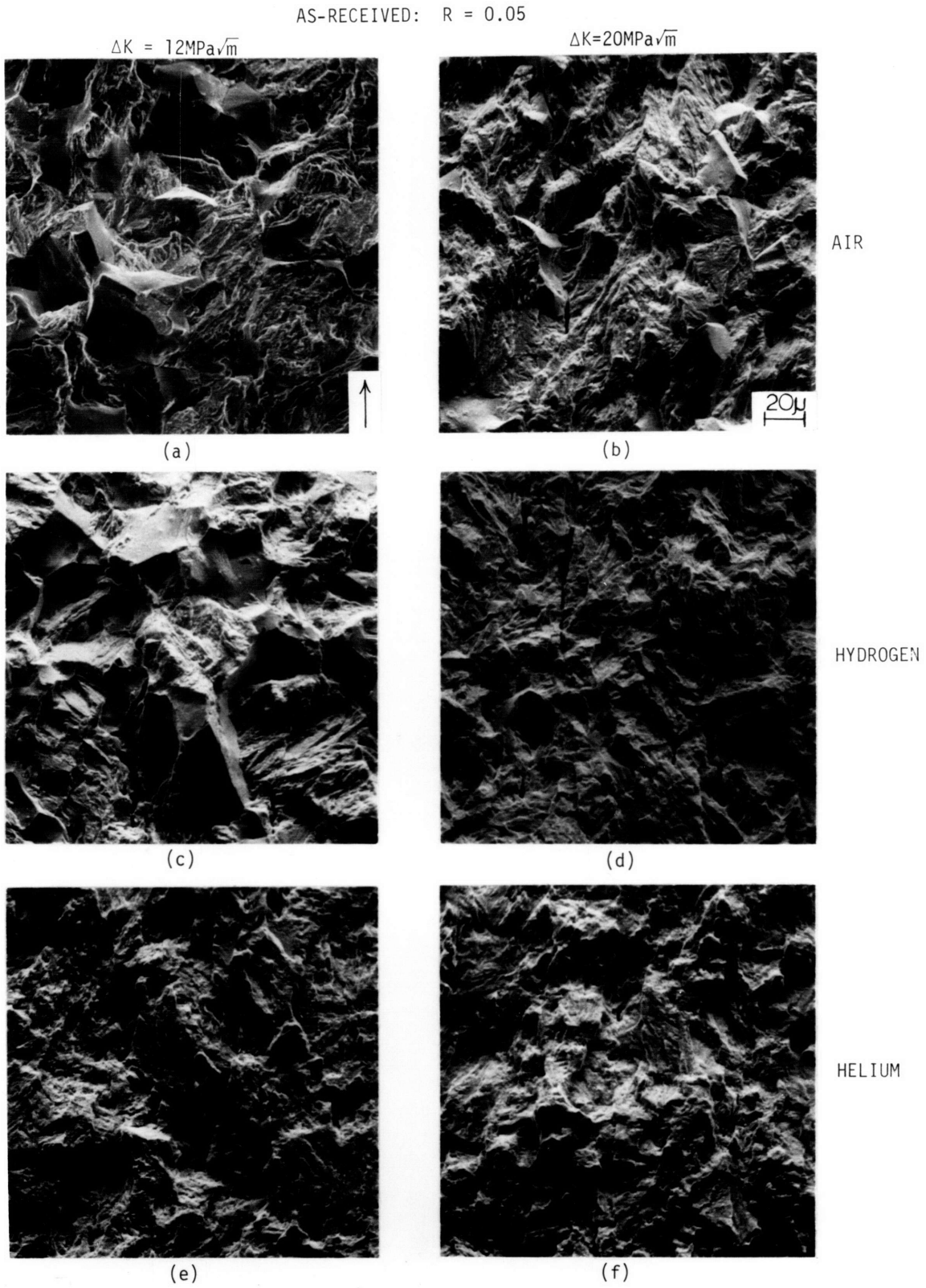

Fig. 20 Comparison of fracture surfaces in air, hydrogen and helium at R = 0.05 for the as-received condition as a function of ΔK.

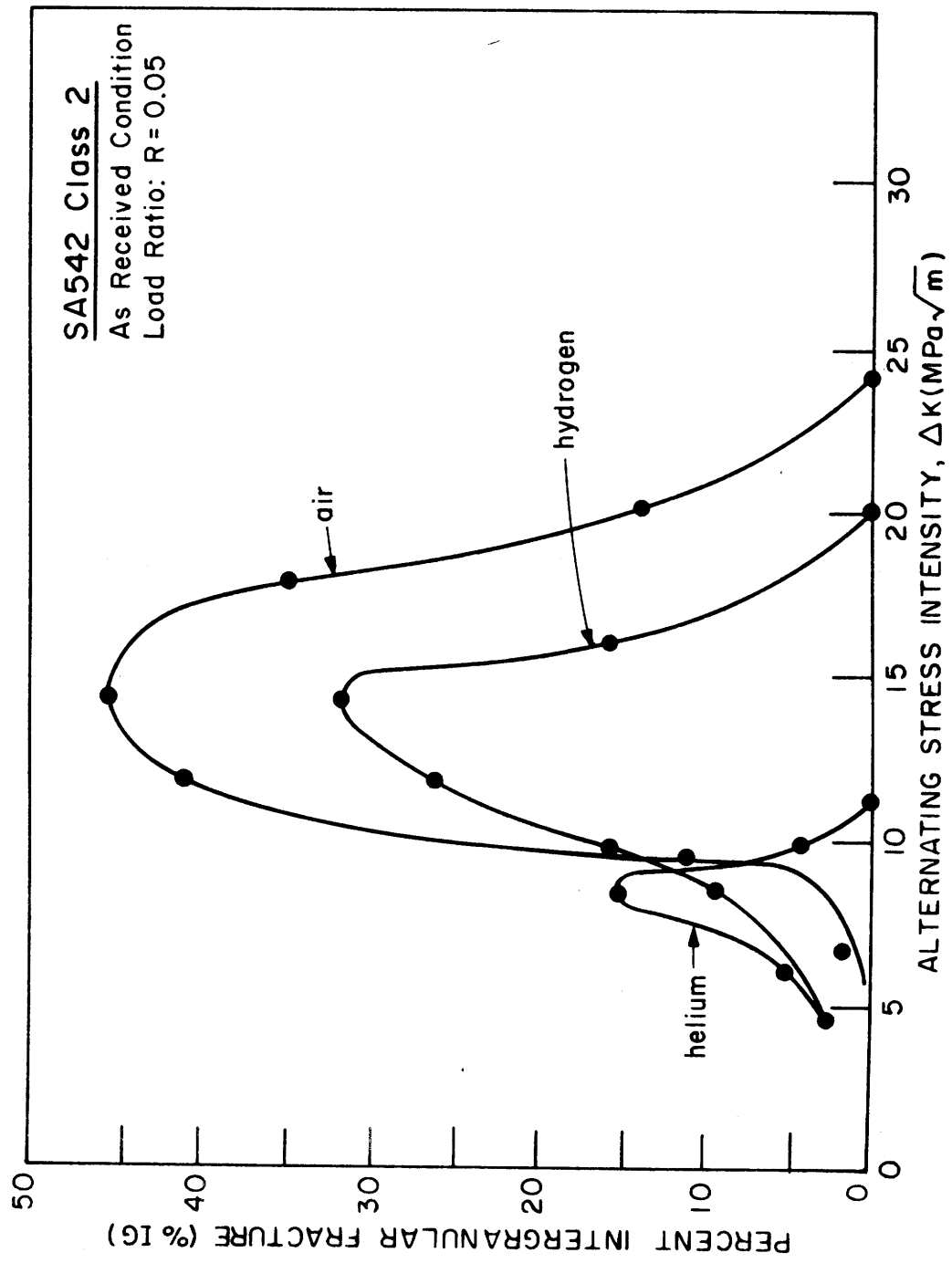

Fig. 21. Variation in percentage of intergranular fracture with alternating stress intensity for the as-received condition in air, hydrogen and helium at R = 0.05.

(ΔK = 8 MPa $\sqrt{m}$). It is interesting to note that the hydrogen and helium environments produced similar near-threshold growth rates (fig. 15), whereas their fracture surfaces are quite different. The air environment test which showed significantly slower near-threshold growth rates, correspondingly displayed the largest fraction of intergranular fracture. This would seem to question whether the percentage of intergranular fracture has an effect on near-threshold growth rates. This is most evident at a ΔK = 14 MPa $\sqrt{m}$, where air and hydrogen show their maximum IG% and helium shows zero IG (Fig. 21), whereas the growth rates of the three tests are similar (varying by less than a factor of 3) at this ΔK (fig. 15).

Fractographs for the as-received condition at a high R (0.75) are shown in figure 22 as a function of environment and ΔK. Tests in hydrogen and helium displayed a finer scale transgranular fracture than those tested in air. The air results showed minimal oxidation compared to low R surfaces, as expected. Air and helium tests showed no IG fracture throughout the tested ΔK range from threshold to 16 MPa $\sqrt{m}$, whereas hydrogen produced a maximum of only 7% at a ΔK = 6 MPa $\sqrt{m}$. These results tend to support evidence that high load ratio tests strongly suppress intergranular cracking in the near-threshold regime (6). Tests at high R, which shows almost identical near-threshold growth

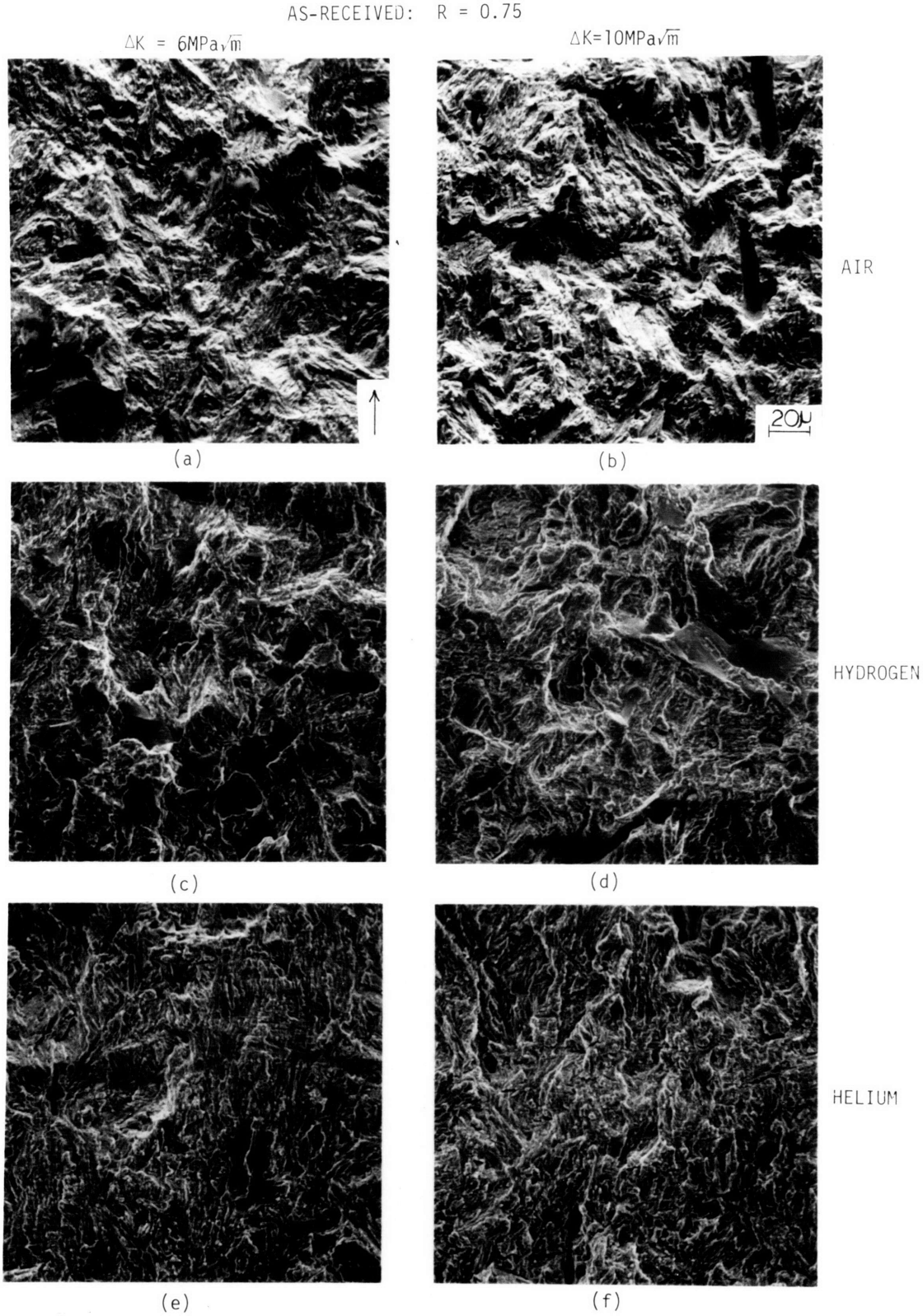

Fig. 22 Comparison of fracture surfaces in air, hydrogen and helium at R = 0.75 for the as-received condition as a function of ΔK.

behavior, shows an absence of IG fracture which is relatively independent of environment. Therefore, intergranular fracture would seem not to be a factor in near-threshold growth at high R.

Fracture surfaces of the 690°C temper were examined, and the pattern of IG fracture was somewhat different than that shown for the as-received condition. Figure 23 compares the 690°C and 320°C temper conditions in air as a function of ΔK. The 690°C temper displays a maximum of 21% IG fracture at ΔK = 20 MPa $\sqrt{m}$. The 320°C temper had 18% IG at ΔK = 12 MPa $\sqrt{m}$, and 15% at ΔK = 20 MPa $\sqrt{m}$. Comparing these results for the 320°C and 690°C conditions in air to the as-received fracture (fig. 24), shows a significantly larger percentage of IG facets (maximum of 46%) for the as-received condition. In this situation the as-received material, which displays a much larger fraction of IG fracture, produced the faster near-threshold growth rates compared to the 690°C temper (fig. 7).

Fracture surfaces of the 690°C temper in hydrogen and helium are shown in figure 25. The helium surfaces exhibited no IG fracture at higher ΔK's and had a maximum of only 5% occurring just above the threshold ΔK_o. A significant variation from the as-received results came from the fracture surfaces of the 690°C tests in hydrogen. The percentage of IG fracture ranged from 4% at near-threshold to a maximum of 63% at a ΔK = 12 MPa $\sqrt{m}$ (fig. 26). Therefore for the 690°C tests, hydrogen displayed

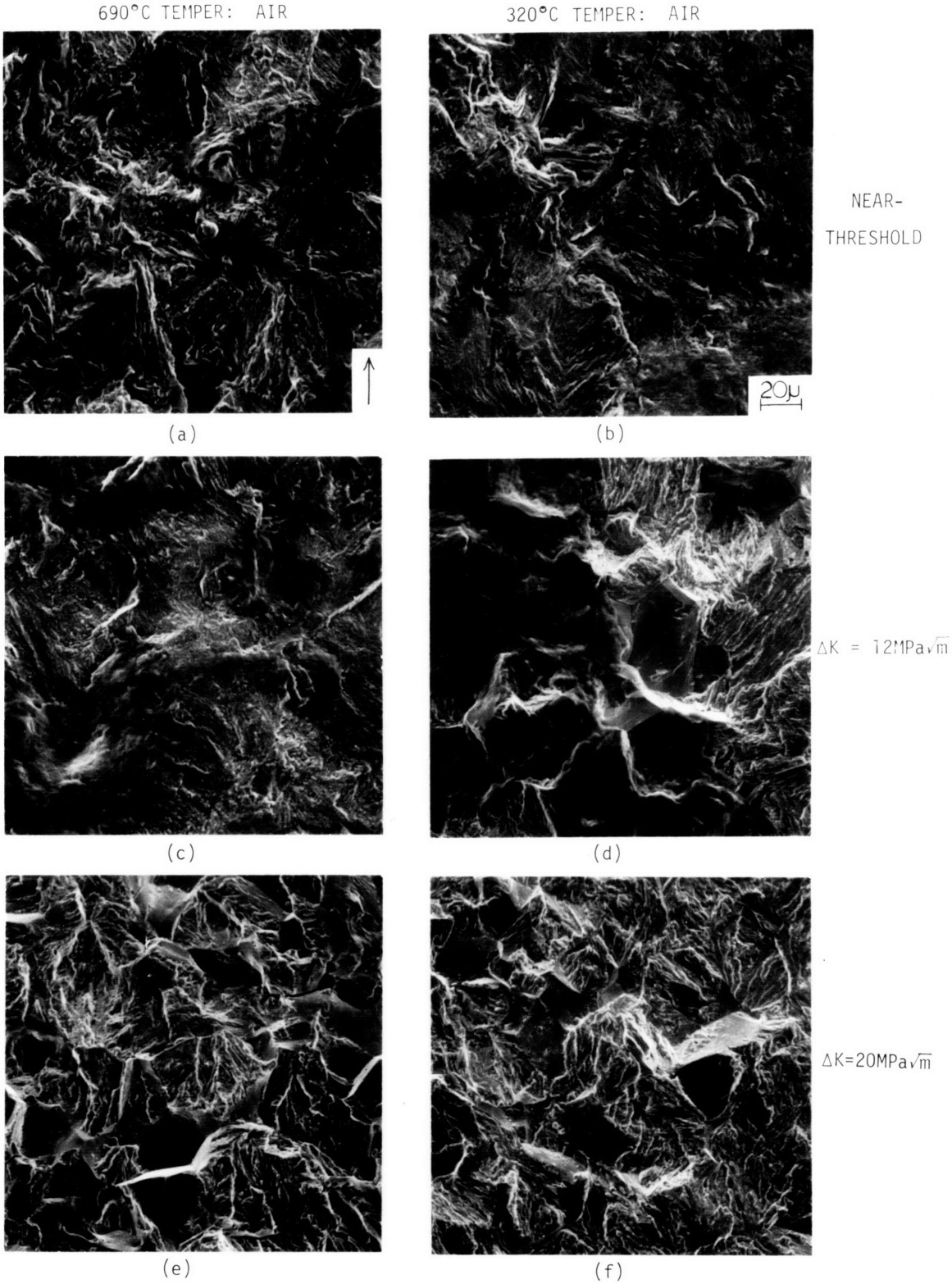

Fig. 23 Comparison of fracture surfaces of the 690°C and 320°C temper conditions in air at R = 0.05 as a function of ΔK.

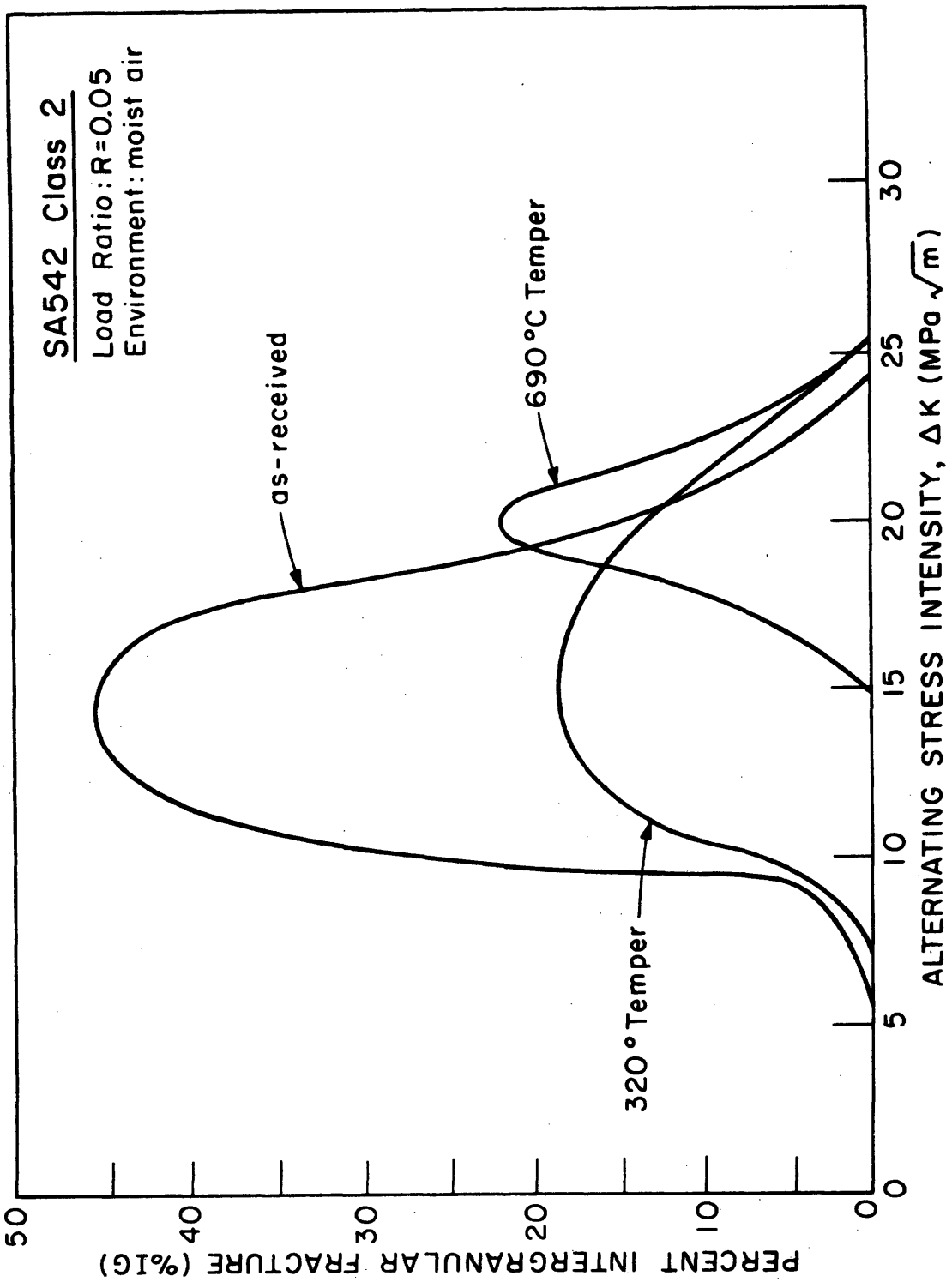

Fig. 24 Variation in percentage of intergranular fracture with alternating stress intensity as a function of material condition for moist air.

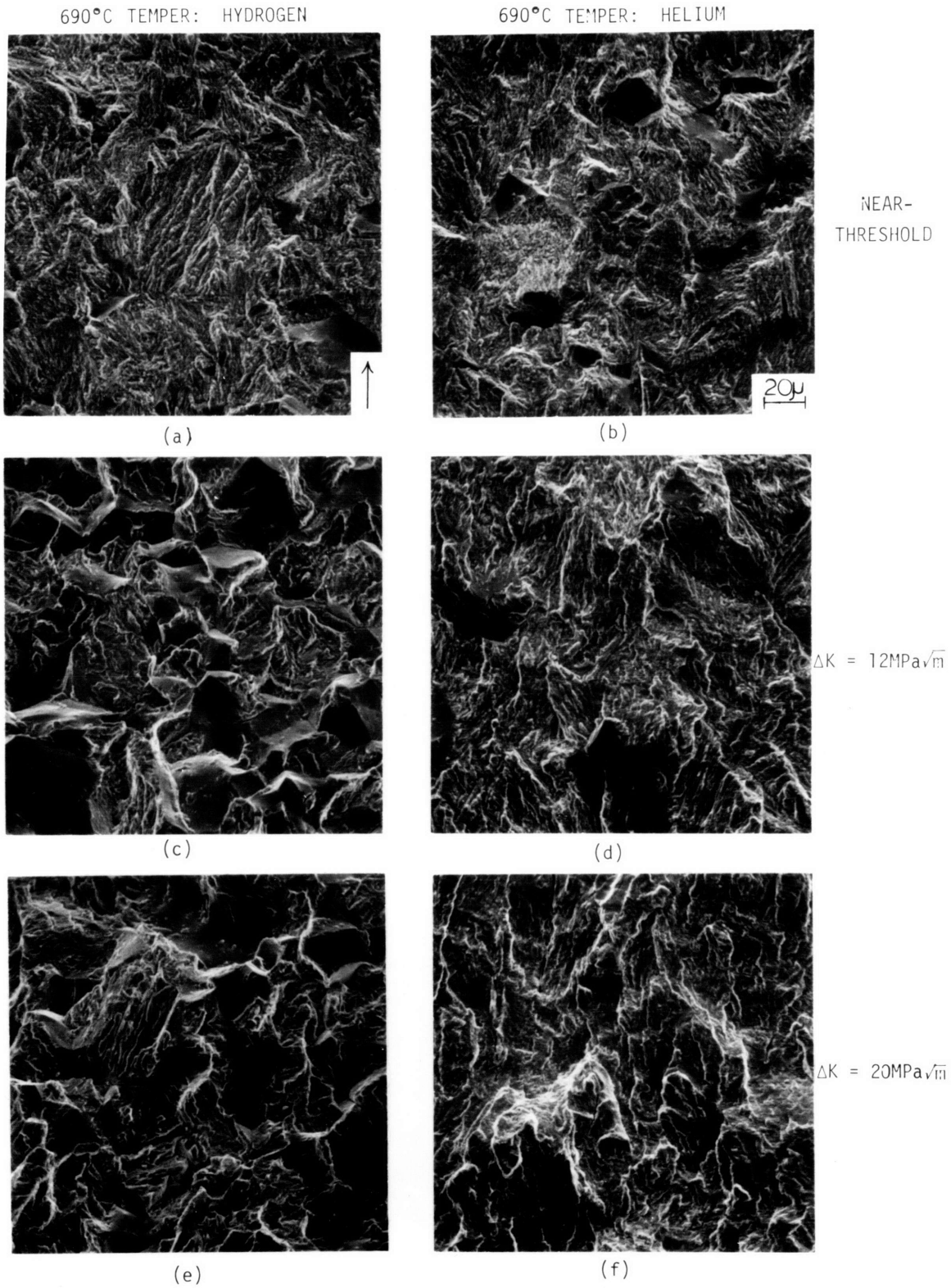

Fig. 25 Comparison of fracture surfaces in hydrogen and helium at R = 0.05 for the 690°C temper condition as a function of ΔK.

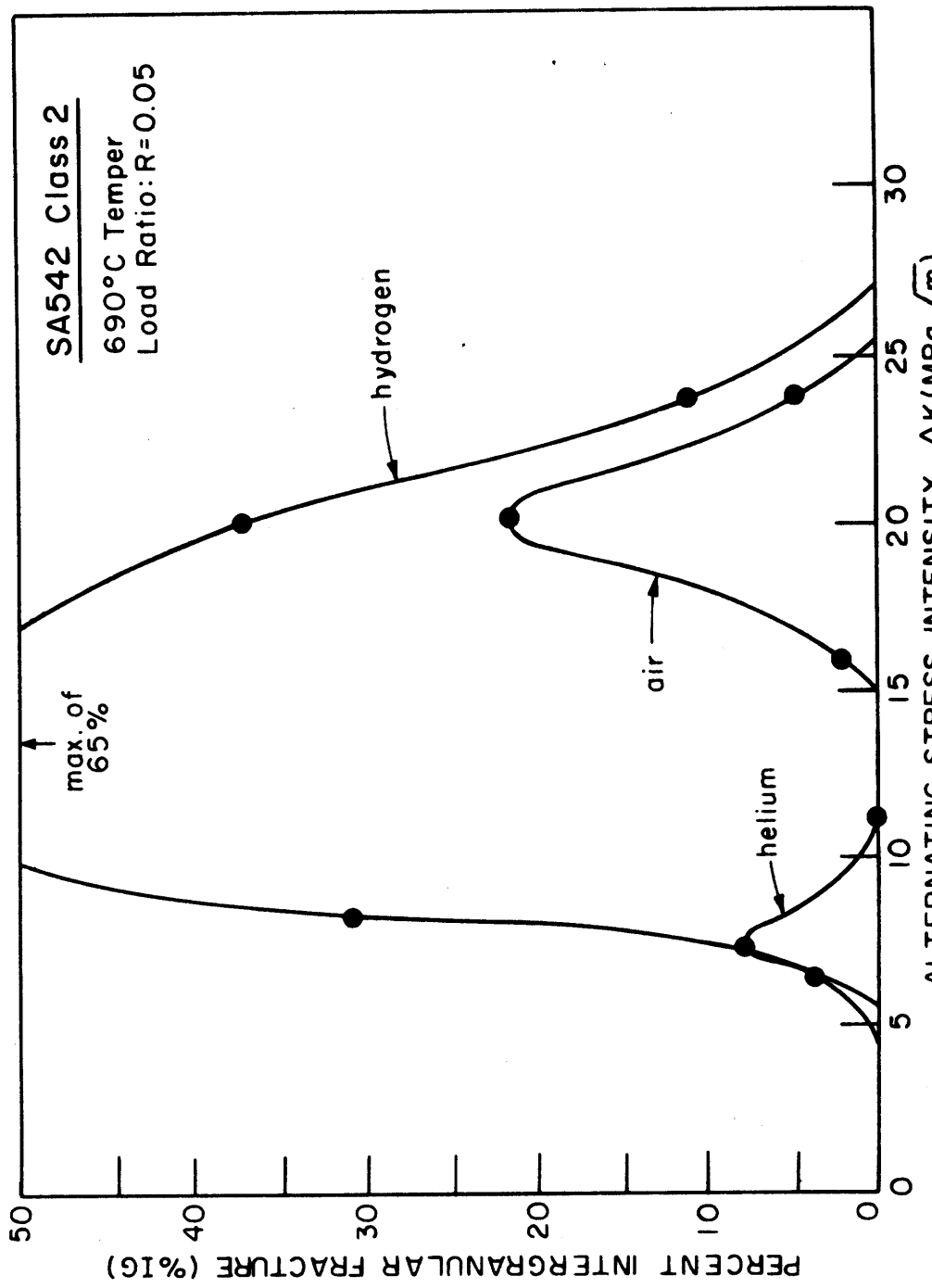

Fig. 26: Variation in percentage of intergranular fracture with alternating stress intensity for the 690°C temper condition in air, hydrogen and helium at R=0.05.

a much larger percentage of IG fracture (63%) compared to air (21%), whereas for the as-received tests the larger percentage was seen in air (46%) relative to the hydrogen (31%) environment (figs. 26 and 27). However for both material conditions, the hydrogen environment enhanced near-threshold growth rates compared to air (fig. 17). The interesting point to be made is that hydrogen produced a larger decrease in the threshold ΔK_o value (35%) for the as-received condition compared to the 690°C temper (19%). Therefore, the larger percentage of IG fracture did not produce a larger increase in near-threshold growth rates. An interesting point for the 690°C temper tests is the very large difference between the helium and hydrogen fracture characteristics (figs. 25 and 26), yet both environments produced almost identical near-threshold behavior (fig. 16).

Therefore, the results found from the fracture surfaces from this phase of the study tend to indicate that the near-threshold growth rates (at low R) may be independent of the relative proportion of intergranular fracture.

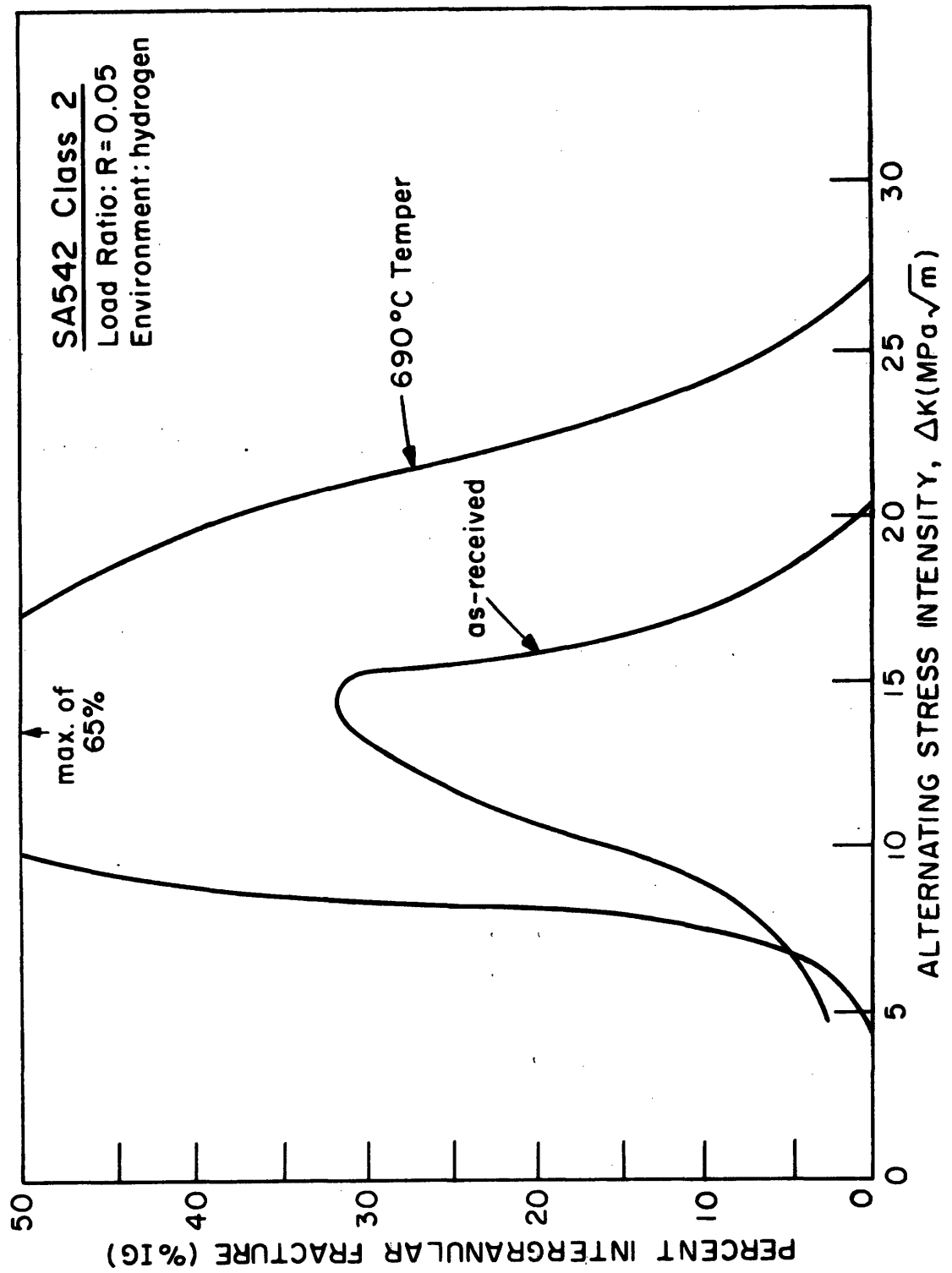

Fig. 27 Variation in percentage of intergranular fracture with alternating stress intensity for the 690°C temper and as-received condition in hydrogen.

CHAPTER IV

DISCUSSION

4.1 PLASTICITY INDUCED CRACK CLOSURE: A MODEL FOR LOAD RATIO EFFECTS

To explain the effect of load ratio on near-threshold behavior (fig. 12), it is important to first recognize results from tests where the load ratio was varied at a number of values between 0.05 and 0.8. Figure 28 is taken from work by Moss(6) on SA387 steel. This curve of threshold ΔK_o versus load ratio R, indicates a trend of decreasing threshold with increasing load ratio. However, once R has obtained a critical value, the threshold ΔK_o remains constant with any further increase in load ratio. Cooke and Beevers (22), and Masounave and Bailon (23) found that this effect of load ratio on threshold ΔK_o, before the critical R, occurred at a constant value of K_{max}. Ritchie (7) observed similar trends in ultra high strength 300M steel. Schmidt and Paris (13) showed that above the critical R, the threshold ΔK_o remains constant whereas K_{max} increases.

A model that may explain this behavior of decreasing ΔK_o for increasing load ratios up to a critical R value, followed by a constant ΔK_o for further increases in R, is based on 'plasticity induced crack closure'. The phenomenon of crack closure was first experimentally detected by Elber (21), who argued that residual plastic deformation left in the wake of a growing crack produces

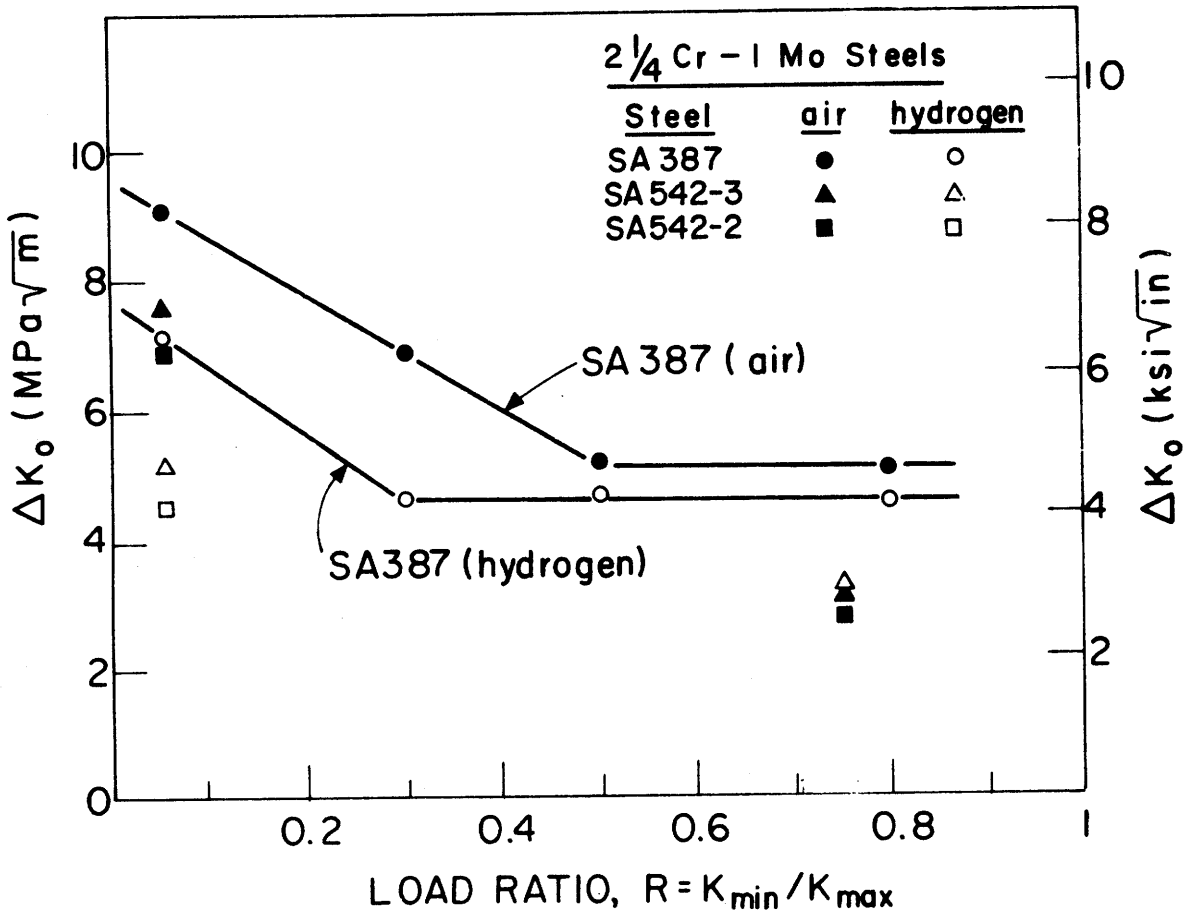

Fig. 28: Variation of threshold ΔKo with load ratio for SA387 steel in moist air and hydrogen (6).

compressive stresses on the fracture surfaces. This can cause the fracture surfaces to come in contact before the tensile loading cycle reaches the minimum load. When the surfaces are in contact, crack growth is nil. Figure 29a is a plot of the alternating stress intensity wave. If the point of fracture surface contact is given a value of '$K_{closure}$' (Kcl in diagram) it can be seen that any part of the ΔK wave below $K_{closure}$ is ineffective in crack propagtion. Therefore, the applied ΔK is reduced to an effective ΔK, the difference being K_{min} subtracted from $K_{closure}$. As $K_{closure}$ increases, the effective ΔK decreases.

As the load ratio R is increased from a low value (eg 0.05), the ΔK curve shifts upward relative to $K_{closure}$. Thus, less of the loading cycle is affected by closure and the effective ΔK approaches the applied ΔK. This perhaps explains why near-threshold growth rates increase, and threshold ΔK_o decreases, as R is increased from a low value. The threshold for crack growth will be reached when the crack remains closed throughout the entire loading cycle. Therefore, with the <u>effective</u> K_{min} (Kcl) not varying with R, the threshold depends on when K_{max} is lowered to the point where the crack does not open. This provides a feasible explanation for the constant K_{max} for low R (fig. 29c).

At the point when K_{min} of the loading cycle has been increased (by increasing R) to $K_{closure}$, the effect of plasticity induced crack closure ceases. This occurs at the critical R value

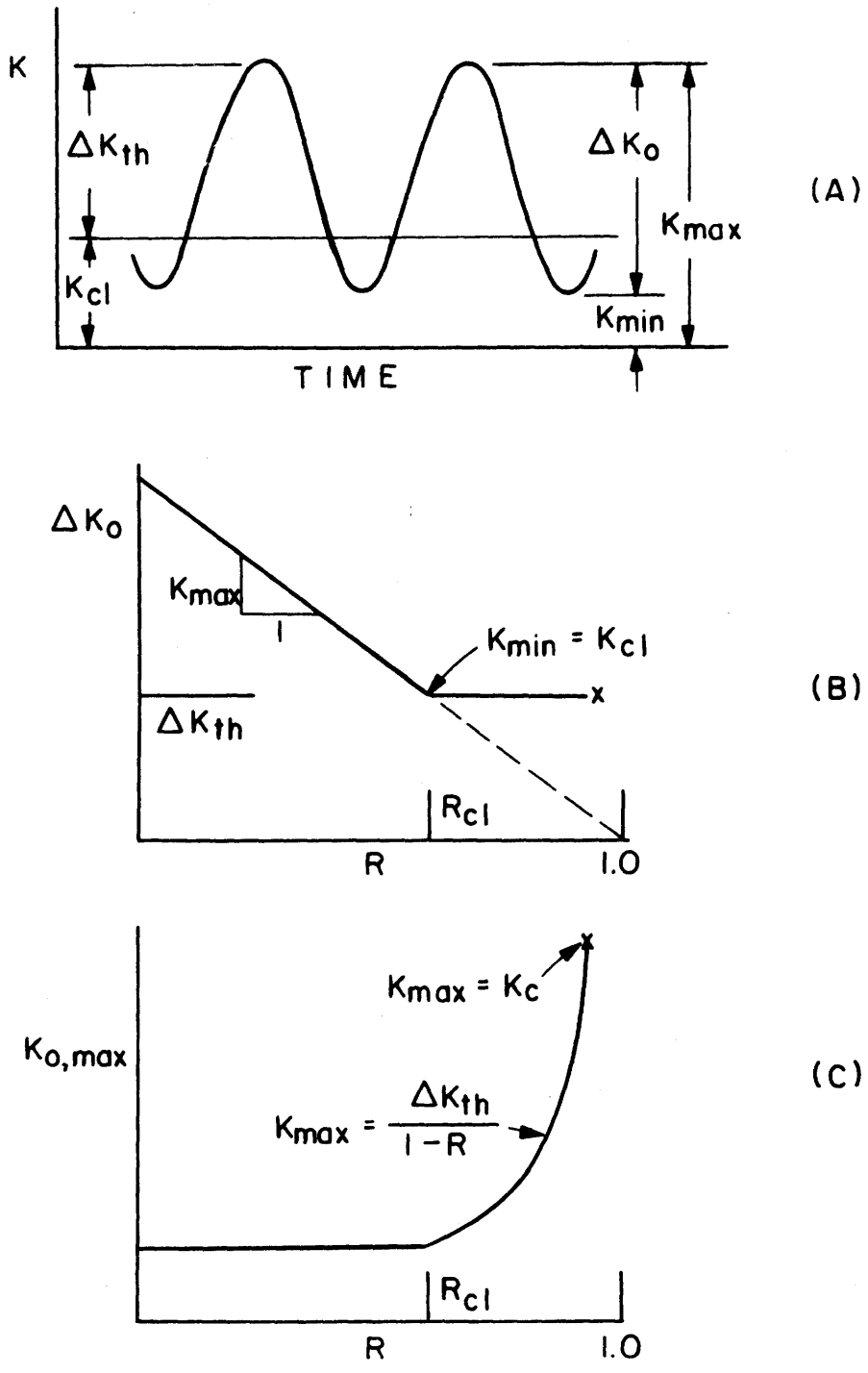

Fig 29 : Nomenclature for stress intensity parameters at threshold and their variation with load ratio R (after Schmidt and Paris)

described earlier. Above this critical R, the fracture surfaces do not come into contact from residual plastic deformation and the applied ΔK equals the effective ΔK. The threshold value is now a function of the ΔK needed to cause crack closure simply by reduction of load. This may explain the constant ΔK_o for high load ratios. However this argument does depend solely on the assumption that the effective ΔK at threshold is constant.

Therefore, the results observed in figure 12 of a decreasing threshold ΔK_o with increasing load ratio R may be explained by 'plasticity induced crack closure'. The behavior of moist air producing the largest change in threshold ΔK_o will be explained below. Further tests on the as-received material are needed so as to fully investigate the effect of R, such as was seen by Moss (fig. 28).

4.2 OXIDE INDUCED CRACK CLOSURE: A MODEL FOR ENVIRONMENTAL EFFECTS

The environmental effects on near-threshold behavior, observed in this study (figs. 15 and 16) displayed results which strongly question previous environmental models, and tend to give strong evidence to a new model.

The hydrogen enhancement of growth in the near-threshold regime was thought to be due to some mechanism of hydrogen embrittlement (HE). There have been many models proposed for HE of high strength steels, with the decohesion model most widely accepted. The decohesion model tends to predict only marginal hydrogen enrichments for low strength steels due to the small magnitude of hydrostatic stress. Many aspects of the results in this study seem to question these HE models. These results are that the enhancement of hydrogen, which is so strong at low R, is nonexistent at high R (fig. 15), the lack of a distinct fracture mode transition, and the similarity of the inert environmental effects to hydrogen.

A model has been proposed (45, 51, 53, 55) that may explain these environmental effects and is based on the concept of 'oxide induced crack closure'. This form of crack closure is based on the observation of microscopic corrosion (oxide) bands on the fracture surface of tests conducted in moist air at low load ratios (28, 45, 55). Such corrosion zones were present in all low R, moist air tests of this study (fig. 30a). White (77)

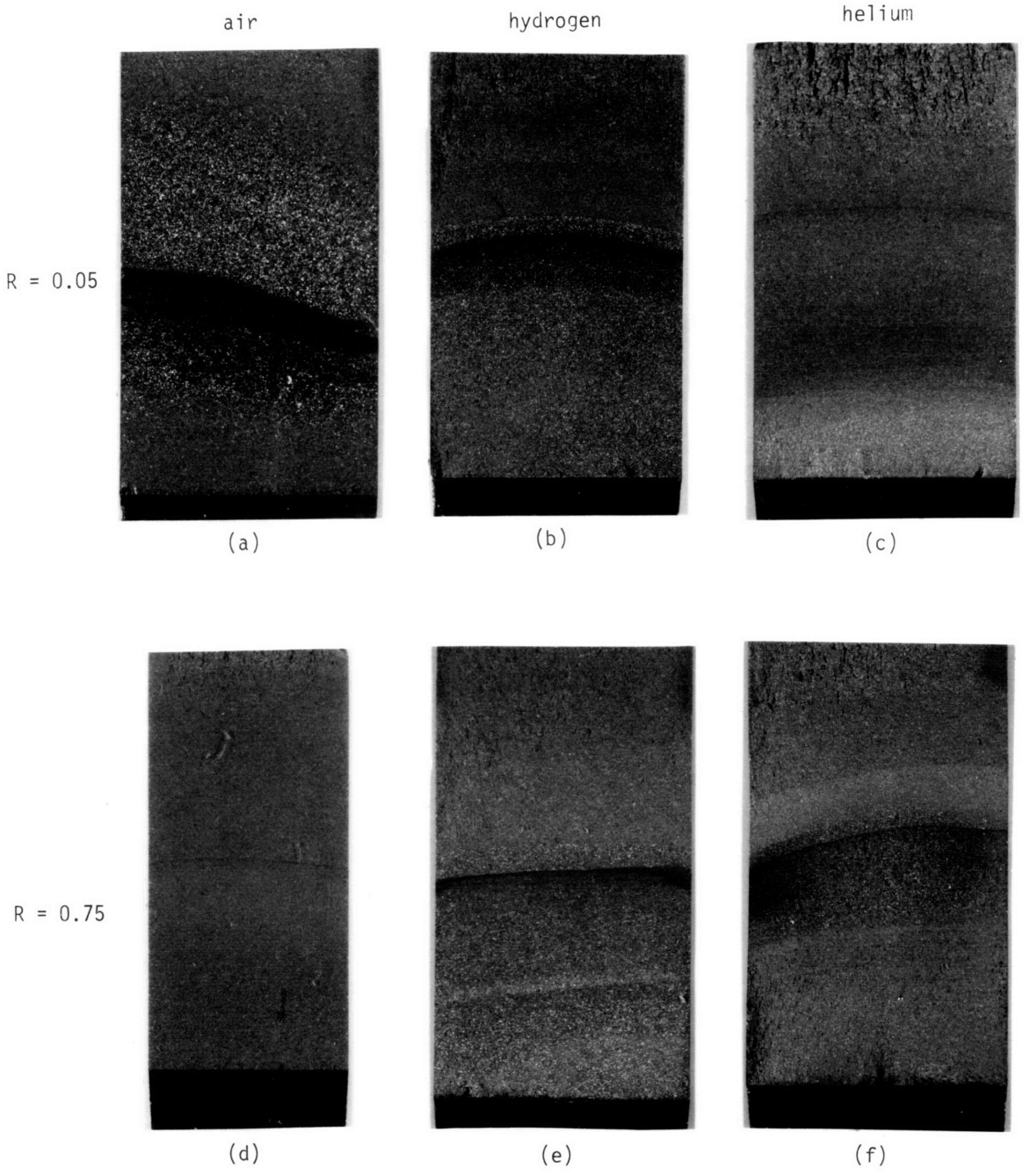

Fig. 30 CT testpiece crack fronts encountered in near-threshold crack growth tests for the as-received material as a function of load ratio and environment (3 1/2 X).

performed Auger measurements of these oxide layers, and the results are shown in figure 31 for a similar steel (SA542-3). Oxide thickness, which is plotted along with the fatigue crack growth rate, is shown to increase with decrease in growth rate, and obtains a maximum value at the threshold growth rate. The maximum oxide thickness corresponds to an increase of almost 30 times that of a naturally formed oxide layer on fresh metal surface, under the same environmental conditions.

A mechanism for this enlarged oxide layer is described by fretting oxidation (51). Once fresh reactive surface is created at the crack tip it will readily oxidize, for tests in moist air. Plasticity induced crack closure, occurring at load ratios below the critical R, causes contact between the two fracture surfaces. The associated tangential friction between the fracture surfaces may lead to cracking of the naturally formed oxide layer. The result is to generate new zones of fresh surface, further oxidation, and a thickening of the oxide film. The reason that the oxide thickness increases with decreasing growth rate has to due with the increased time for fretting oxidation to occur. At high load ratios there is no plasticity induced crack closure. Therefore for tests in moist air, where there will exist a naturally formed oxide layer, there is no mechanism for increased oxidation.

The significance of this oxide build up at near-threshold growth rates (for low R) is to <u>increase</u> crack closure. Contact

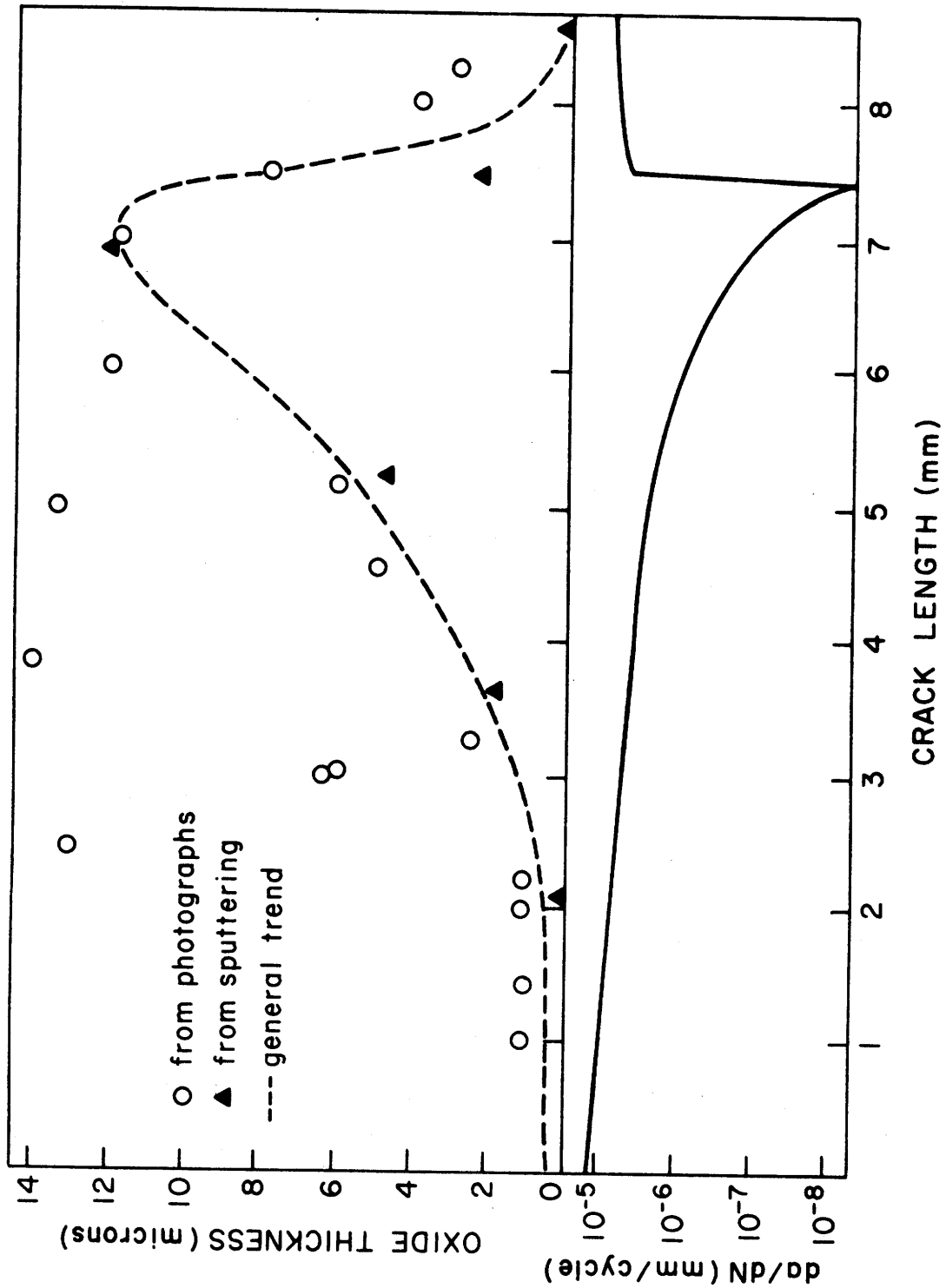

Fig. 31 Oxide thickness and crack propagation along crack for SA542-3 at R = 0.05 in moist air (courtesy of C.M. White).

of the two fracture surfaces will occur sooner, thereby increasing closure initiation, increasing $K_{closure}$, and therefore decreasing the effective ΔK. Purified hydrogen and helium tests show relatively no evidence of oxidation (fig. 30), therefore there would be no mechanism for increased closure by oxide buildup.

The oxide induced crack closure model proposes that the large influence of hydrogen on the near-threshold regime (compared to moist air) may not be due to hydrogen enhancing growth, but rather to the moist air environment decreasing growth due to oxide buildup. This model seems to explain the almost identical behavior for tests at high load ratio in air, hydrogen and helium, where there is no crack closure mechanism in operation except closure from reducing the loads to threshold ΔK_0.

This model may not explain the variation of intergranular fracture among the different environments at low R, but it could possibly explain the independence of the near-threshold growth rates on the proportion of intergranular fracture. This independence could be due to the fact that the mechanism is a surface phenomenon.

Also, the similarity of near-threshold growth rates for hydrogen and helium at low R can be explained by the fact that both environments are relatively void of moisture and oxygen. The enlarged oxide layer may explain the larger effect of load ratio R on the threshold ΔK_0 for tests in moist air (fig. 12).

Only one test point plotted (air, low R) in this figure exceeds the general trend, and this point would be the only one affected by oxide induced crack closure (which explains an increase in threshold ΔK_o). Therefore, this model of oxide induced crack closure seems to be qualitatively consistent with experimental observations.

If this model is correct, then for applications which contain dry atmospheres (including dry hydrogen), the addition of small traces of moisture/oxygen could significantly reduce near-threshold growth of small flaws.

4.3 CONCLUDING REMARKS

This study of fatigue behavior of SA542 class 2 steel was initiated to analyze and record what effect certain application oriented factors would have on near-threshold crack growth.

The results of this study have shown that the near-threshold growth regime can produce significant growth rates; especially for applications with high load ratios, dry operating environments at low load ratios and for materials of higher yield strengthes. The study correspondingly showed that low load ratios, moist/oxygenated environments and lower strength materials lowered near-threshold growth rates.

These results (table II) may help the material design of flaw critical applications where the lifetime to propagate subcritical flaws is a high priority characteristic, especially when environmental effects may be present.

Future work that may add to the present study includes:

1) investigating the effect of load ratio over a wider range of values to observe if it fulfills the plasticity induced crack closure arguments, as to a critical load ratio.

2) testing a range of yield strength values with the intent of directing the work at a model for the strength effects.

3) investigation into possible fracture mechanisms that could explain the seemingly unrelated variation of intergranular fracture with near-threshold growth rates.

HEAT TREATMENT	σ_{YS}	ENVIRONMENT	R	ΔK_o	K_{max}	CYCLIC PLASTIC ZONE SIZE	MAXIMUM PLASTIC ZONE SIZE	CYCLIC CTOD[1]	MAXIMUM CTOD[2]
(°C)	(MPa)		Kmin/ Kmax	(MPa$\sqrt{m}$)	(MPa$\sqrt{m}$)	(μm)	(μm)	(μm)	(μm)
AS RECEIVED	769	MOIST AIR	0.05	7.1	7.5	3.4	15.1	0.08	0.17
AS RECEIVED	769	MOIST AIR	0.75	2.8	11.2	0.5	33.7	0.01	0.41
AS RECEIVED	769	UHP HYDROGEN	0.05	4.6	4.8	1.4	6.2	0.03	0.07
AS RECEIVED	769	UHP HYDROGEN	0.75	2.8	11.2	0.5	33.7	0.01	0.38
AS RECEIVED	769	UHP HELIUM	0.05	4.9	5.2	1.6	7.3	0.04	0.08
AS RECEIVED	769	UHP HELIUM	0.75	2.7	10.8	0.5	31.4	0.01	0.35
690°C TEMPER	575	MOIST AIR	0.05	8.6	9.1	8.9	39.9	0.15	0.34
690°C TEMPER	575	UHP HYDROGEN	0.05	6.9	7.3	5.7	25.7	0.10	0.22
690°C TEMPER	575	UHP HELIUM	0.05	7.1	7.5	6.1	27.1	0.10	0.23
320°C TEMPER III	951	MOIST AIR	0.05	7.6	7.9	3.9	11.0	0.07	0.15
320°C TEMPER III	951	UHP HYDROGEN	0.05	6.0	6.3	1.6	7.0	0.04	0.10

Table II. Summary of fatigue crack growth test parameters and the corresponding threshold ΔK_o values for the SA542 class 2 steel.

CHAPTER V

CONCLUSIONS

This study of the factors affecting near-threshold fatigue crack propagation in SA542 class 2 (2 1/4 Cr - 1 Mo) steel has shown:

1) Laboratory heat treatment of the thin plate SA542 class 2 steel included austenitizing (950°C), quenching and tempering (320°C - 690°C). These treatments produced a variation in yield strength from 575 MPa to 951 MPa. Microstructures were fully martensitic with a prior austenite grain size of 40 μm.

2) Near-threshold growth rates are increased by up to 100 times with an increase in yield strength from 575 MPa to 769 MPa. Threshold ΔK_o values were decreased by 17% from 8.6 MPa $\sqrt{m}$ to 7.1 MPa $\sqrt{m}$ in moist air for the same strength increase.

3) The effect of increasing the load ratio from 0.05 to 0.75 for the as-received material (769 MPa) tested in moist air was to reduce the threshold ΔK_o by 60% from 7.1 MPa $\sqrt{m}$ to 2.8 MPa $\sqrt{m}$. Near-threshold growth rates were increased by up to 3 orders of magnitude. Tests under the same conditions in helium, showed a reduction in threshold ΔK_o from 4.9 MPa $\sqrt{m}$ to 2.7 MPa $\sqrt{m}$, while tests in hydrogen showed threshold reduction from 4.6 MPa $\sqrt{m}$ to 2.8 MPa $\sqrt{m}$.

4) The effect of load ratio is consistent with concepts of plasticity induced crack closure. This closure effect reduces

the applied alternating stress intensity. Closure is most significant at low load ratios, and the effect decreases with increasing load ratio. Upon reaching a critical R value, crack closure ceases. This model may explain the decreasing threshold ΔK_o values with increasing R up to the critical R, and the subsequent constant ΔK_o values above critical R.

5) Environmental tests on the as-received material presented a situation where at low R, the effect of UHP hydrogen and UHP helium was to increase near-threshold growth rates in a similar manner compared to moist air. Hydrogen produced a ΔK_o of 4.6 MPa $\sqrt{m}$ and helium a value of 4.9 MPa $\sqrt{m}$ compared to a moist air value of 7.1 MPa $\sqrt{m}$. Tests at high R showed all three environments having almost identical near-threshold behavior with ΔK_o values of 2.7 MPa $\sqrt{m}$ for helium and 2.8 MPa $\sqrt{m}$ for hydrogen and air. Tests on the 575 MPa strength displayed similar trends, where at low R (0.05) the threshold values were 8.6 MPa $\sqrt{m}$ for air, 7.1 MPa $\sqrt{m}$ for helium and 6.9 MPa $\sqrt{m}$ for hydrogen. The results seemed to question the hydrogen embrittlement mechanism. A new model that tends to explain these results is 'oxide induced crack closure'. This model is based on measurements showing an increased oxide layer on the fracture surfaces for tests in moist air at locations of near-threshold growth. This increased oxide layer (30x a naturally formed layer) is explained by fretting oxidation, whereby crack closure of the surfaces causes oxide cracking,

reoxidation and thus a buildup of oxide. The effect of this oxide is to increase closure and decrease near-threshold growth rates. This model states that the large difference in near-threshold growth rates is not due to hydrogen (or helium) increasing growth, but rather to moist air slowing up growth.

6) Mid growth regimes, at the frequency of 50 Hz used, were relatively independent of load ratio, material strength and environment, except that the inert helium did show slower growth rates.

7) Fracture surfaces showed a predominantly fine scale transgranular mode with varying percentages of IG fracture. Tests for the as-received material at low R (0.05) displayed maximum percentages of 46% for air, 31% for hydrogen and 14% for helium. Whereas for tests on the 690°C temper at low R (0.05), hydrogen displayed a maximum of 63%, 21% for air and 5% for helium. Tests at high R (0.75) on the as-received material showed no IG fracture for air or helium, and a maximum of only 7% for hydrogen.

The main conclusion of the fractography is that the near-threshold growth behavior seems to be quite independent of the appearance of intergranular fracture. The oxide induced crack closure model may explain this independence because this model is based on surface phenomena.

REFERENCES

1. Ritchie, R.O., "Investigation of Factors Affecting Near-Threshold Fatigue Crack Growth in Low Alloy, Pressure Vessel Steels", Quarterly Report Nos. 1-7 for DOE.

2. Srawley, J.E., Intl. J. of Fracture, Vol. 12, 1976, p. 475.

3. Landes, J.D., and McCabe, D.E., "Design Properties for Coal Conversion Vessels", Quarterly Report Nos. 1-6 for EPRI.

4. Ritchie, R.O., "Environment Sensitive Fracture of Engineering Materials", Z. A. Foroulis, ed., p. 538, TMS-AIME, Publ. 1979.

5. Ritchie, R.O., Metal Science, Vol. 11, 1977 p. 368

6. Moss, C.M., "Near-Threshold Fatigue Crack Propagation in Pressure Vessel Steel", S.M. Thesis, Massachusetts Institute of Technology, Sept. 1979.

7. Ritchie, R.O., Journal of Engineering Materials and Technology, Transactions of the Americal Society of Mechanical Engineers, Series H, vol. 99, 1977, p. 195.

8. Brazil, R.L., Simmons, G.W., and Wei, R.P., "Fatigue Crack Growth in 2 1/4 Cr - 1 Mo Steel exposed to Hydrogen Containing Gases", Journal of Engineering Materials and Technology, Trans. of ASME, Series H, Vol. 101, 1979.

9. Masounave, J. and Bailon, J.P., Scripta Metallurgica, Vol. 10, 1976, p. 165.

10. Pook, L.P., ASTM STP 513, Americal Society for Testing and Materials, 1972, p. 106.

11. Beevers, C.J., Metal Science, Vol. 11, 1977 p. 362.

12. Knott, J.F., and Pickard, A.C., Metal Science, Vol. 11, 1977, p. 399.

13. Schmidt, R.A., and Paris, P.C., "Progress in Flaw Growth and Fracture Toughness Testing", ASTM STP 536, 1973 p. 79.

14. Masounave, J., and Bailon, J.P., Scripta Metallurgica, Vol. 10, 1976, p. 165.

15. Carlson, M.F., and Ritchie, R.O., Scripta Metallurgica, Vol. 11, 1977, p. 1113

16. Ritchie, R.O. and Bathe, K.J., International Journal of Fracture Vol. 15, 1979 p. 47.

17. Aronson, G.H. and Ritchie, R.O., Journal of Testing and Evaluation, Vol. 7, 1979.

18. Pelloux, R.M.N., Engineering Fracture Mechanics, Vol. 1, 1970, p. 697.

19. Ritchie, R.O., and Knott, J.F., Materials Science and Engineering, Vol. 14, 1974, p. 7.

20. Beevers, C.J., Cooke, R.J., Knott, J.F., and Ritchie, R.O., Metal Science, Vol. 9, 1975, p. 119.

21. Elber, W., "Damage Tolerance in Aircraft Structures", ASTM STP 486, 1971, p. 230.

22. Cooke, R.J., and Beevers, C.J., Engineering Fracture Mechanics, Vol. 5, 1973, p. 1061.

23. Masounave, J. and Bailon, J.P., Scripta Metallurgica, Vol. 9, 1975, p. 723.

24. Ritchie, R.O., Moss, C.M. and Zamiski, G.F., "Investigation of Factors Affecting Near-Threshold Fatigue Crack Growth in Low Alloy Pressure Vessel Steels", M.I.T., Fatigue and Plasticity Laboratory, Feb. 1979.

25. Lindley, T.C., Richards, C.E. and Ritchie, R.O., Metallurgia and Metal Forming, Vol. 43, 1976, p. 268.

26. Vosikovsky, O., Engineering Fracture Mechanics, Vol. 11, 1979, p. 595.

27. Ritchie, R.O., Journal of Engineering Materials and Technology, Trans. ASME, Series H, Vol. 99, 1977, p. 195.

28. Ritchie, R.O., "Near-Threshold Fatigue Crack Propagation in Steels", MIT Fatigue and Plasticity Laboratory.

29. Cooke, R.J. and Beevers, C.J., Materials Science and Engineering, Vol. 13, 1974, p. 201.

30. Cooke, R.J., Irving, P.E., Booth, G.S., and Beevers, C.J., Engineering Fracture Mechanics, Vol. 7, 1975, p. 69.

31. Benson, J.P., and Edmonds, D.V., Metal Science, Vol. 12, 1978, p. 223.

32. McEvily, A.J. "On Notch Sensitivity and the Threshold Level", Monograph, Recent Research on Mechanical Behavior of Solids, University of Tokyo Press, Tokyo, Japan, 1979.

33. Ritchie, R.O., Garrett, G.G. and Knott, J.F., Intl. J. of Fracture Mech., Vol. 7, 1971, p. 462.

34. Ritchie, R.O., "Crack Growth Monitoring: Some Considerations of the Electrical Potential Method", Dept. of Metallurgy and Materials Science Report, University of Cambridge, Jan. 1972.

35. Oriani, R.A., and Josephic, P.H., Acta Metallurgica, Vol. 22 1974, p. 1065.

36. Garber, R., Bernstein, I.M., and Thompson, A.W., Scripta Metallurgica, Vol. 10, 1976, p. 341.

37. Baker, R.G. and Nutting, J., J. Iron and Steel Inst., Vol. 177, 1959, p. 257.

38. Wei, R.P. and Simmons, G.W., "Fracture Mechanics and Surface Chemistry Studies of Steels for Coal Conversion Systems", Annual Reports Nos. 1-2 for Doe, Dec. 1977 - Dec. 1978 Lehigh University.

39. Brown, R.M., Rege, R.A., and Spaeder, Jr. C.E., "The Properties of Normalized and Tempered and of Quenched and Tempered 6 1/4 inch Thick Plates of 2 1/4 Cr - 1 Mo Steel", U.S. Steel Applied Research Labs.

40. Bucci, R.J., Paris, P.C., and Clark, W.G., in Stress Analysis and Growth of Cracks, ASTM STP 513, 1972, pp. 177-195.

41. Beachem, C.D., Metallurgical Transactions, Vol. 3, No. 2, Feb. 1972, pp. 437-451.

42. Cialone, H. and Asaro, R.J., Metallurgical Transactions A, Vol. 10A, No. 3, March 1979, pp. 367-375.

43. Wei, R.P., and Landes, J.D., Mater. Res. Stds., 9, 1969 p.25.

44. Austen, I.M. and McIntyre, P., Metal Science, 13, 1969, p. 25.

45. Ritchie, R.O., Suresh, S. and Toplosky, J., "Influences of Gaseous Environment on Low Growth-Rate Fatigue Crack Propagation in Steels", Annual Report No. 1 for Doe, Jan. 1980.

46. Irving, P.E. and Beevers, C.J., Met. Trans. A, Vol. 5, 1975, p. 391.

47. McEvily, A.J., Metal Science, Vol. 11, 1977, p. 274.

48. Paris, P.C., Bucci, R.J., Wessel, E.T., Clark, W.G. and Mager, T.R., ASTM STP 513, 1972 p. 141.

49. Tu, L.K.L. and Seth, B.B., J. Test. Eval., Vol. 6, 1978. p. 66.

50. Wei, R.P. and Landes, J.D., Mater. Res. Stds., Vol. 9, 1969, p. 25.

51. Stewart, A.T., Eng. Fract. Mech., 1980.

52. Ritchie, R.O., Intl. Metals Reviews, Vol. 20, 1979, p. 205.

53. Suresh, S., Zamiski, G.F., and Ritchie, R.O., "Fatigue Crack Propagation Behavior of 2 1/4 Cr - 1 Mo Steels for Thick Wall Pressure Vessels", in The Application of 2 1/4 Cr - 1 Mo Steels for Thick Wall Pressure Vessels", ASTM STP, ASTM, 1980.

54. Suresh, S., Moss, C.M., and Ritchie, R.O., "Hydrogen-Assisted Fatigue Crack Growth in 2 1/4 Cr - 1 Mo Low Strength Steels", Trans. Japan Instit. of Metals, Vol. 21, 1980, p. 481.

55. Ritchie, R.O., Moss, C.M., and Suresh, S., Journal of Engineering Materials and Technology, Trans. of ASME, Series H, Vol. 102, 1980.

56. Paris, P.C., Bucci, R.J., Wessel, E.T., Clark, W.G., and Mager, T.R., ASTM STP 513, 1972, p. 141.

57. Fine, M.E., and Ritchie, R.O., "Fatigue Crack Initiation and Near-Threshold Crack Growth, "Fatigue and Microstructure" p. 245 (ASM 1979).

58. Horn, R.M., Parker, E.R. and Zackay, V.F., "Low Alloy Steels for Thick Wall Pressure Vessels", University of California-Berkeley 1977.

59. Wilson, R., "Metallurgy and Heat Treatment of Tool Steels" McGraw Hill, 1975.

60. Budiansky, B., and Hutchinson, J.W., "Analysis of Closure in Fatigue Crack Growth", Journal of Applied Mechanics, Vol. 45, No. 2, June 1978.

61. Gangloff, R.P, "Gaseous Hydrogen Embrittlement of High Strengh Steel", Doctoral Thesis, 1974, Lehigh University.

62. Van Atta, C.M., "Vacuum Science and Engineering", McGraw Hill, 1965.

63. Farkass, I. and Barry, E.J., "1960 Vacuum Symposium Transactions" Pergamon Press, 1961.

64. Parker Hannifin Corp., "O-Ring Handbook", Dec. 1977.

65. Roth, A., "Vacuum Technology", North-Holland, 1976.

66. Pirani, M. and Yarwood, J., "Principles of Vacuum Engineering" Reinhold, 1961.

67. Robinson, N.W., "The Physical Principles of Ultra-High Vacuum Systems and Equipment", 1968.

68. Spotts, M.F., "Design of Machine Elements", Prentice Hall, 4th Edition.

69. Brazil, R., Personal Communication Lehigh University, 1979.

70. Gangloff, R.P. and Wei, R.P., "Gaseous Hydrogen Embrittlement of High Strength Steels" Met. Trans. 1977 Vol. 8A, p. 1044.

71. Stern, S.A., Mullhaupt, J., Hempstreet, R., and DiPaulo, F.S., J. Vac. Sci. Technol., 1965, Vol. 2, p. 165.

72. Dandridge, P., Personal Communication, Atomic Ltd Inc., Cambridge, Ma., 1979.

73. Hawkins, G.W., Personal Communication, Dept. of Mechanical Engineering, MIT, 1979.

74. Michmerhuizen, R., Personal Communication, Service Coordinator Varian, 1979.

75. Hoffman, D.M., "Operation and Maintenance of a Diffusion Pumped Vacuum System". J. Vac. Sci, Technol. 16 (1)

Jan., 1979 pp. 71-74

76. Irving, P.E. and Kurzfeld, A., Metal Science, Vol. 12, 1978, p. 495

77. White, C., "Oxide-Induced Crack Closure of Near-Threshold Fatigue Cracks", S.B. thesis, M.I.T., May 1980.

APPENDIX A

ENVIRONMENTAL CHAMBER SYSTEM

It has become increasingly important to define the effect of a purified environment on the near-threshold fatigue growth regime for steels. Therefore an environmental chamber system has been designed that will isolate the crack propagating zone with an ultra high purity gas atmosphere. To obain such a clean system, the design criteria has been based on high vacuum standards. The goal of the system is to produce an impurity level of less than 1ppm.

A complete schematic of the environmental chamber system is shown in figure 32. The principle operating characteristics of this chamber system includes:

1) Bake out at approximately 100°C during an inert environment purge.
2) Evacuation to a pressure of approximately 5 millitorr by a mechanical roughing system and a cryogenic impurity adsorbing pump.
3) Pressurization with an ultra high purity (UHP) gas which flows through an oxygen catalytic converter, a moisture adsorbing molecular sieve and a liquid nitrogen coil trap, prior to entering the chamber.

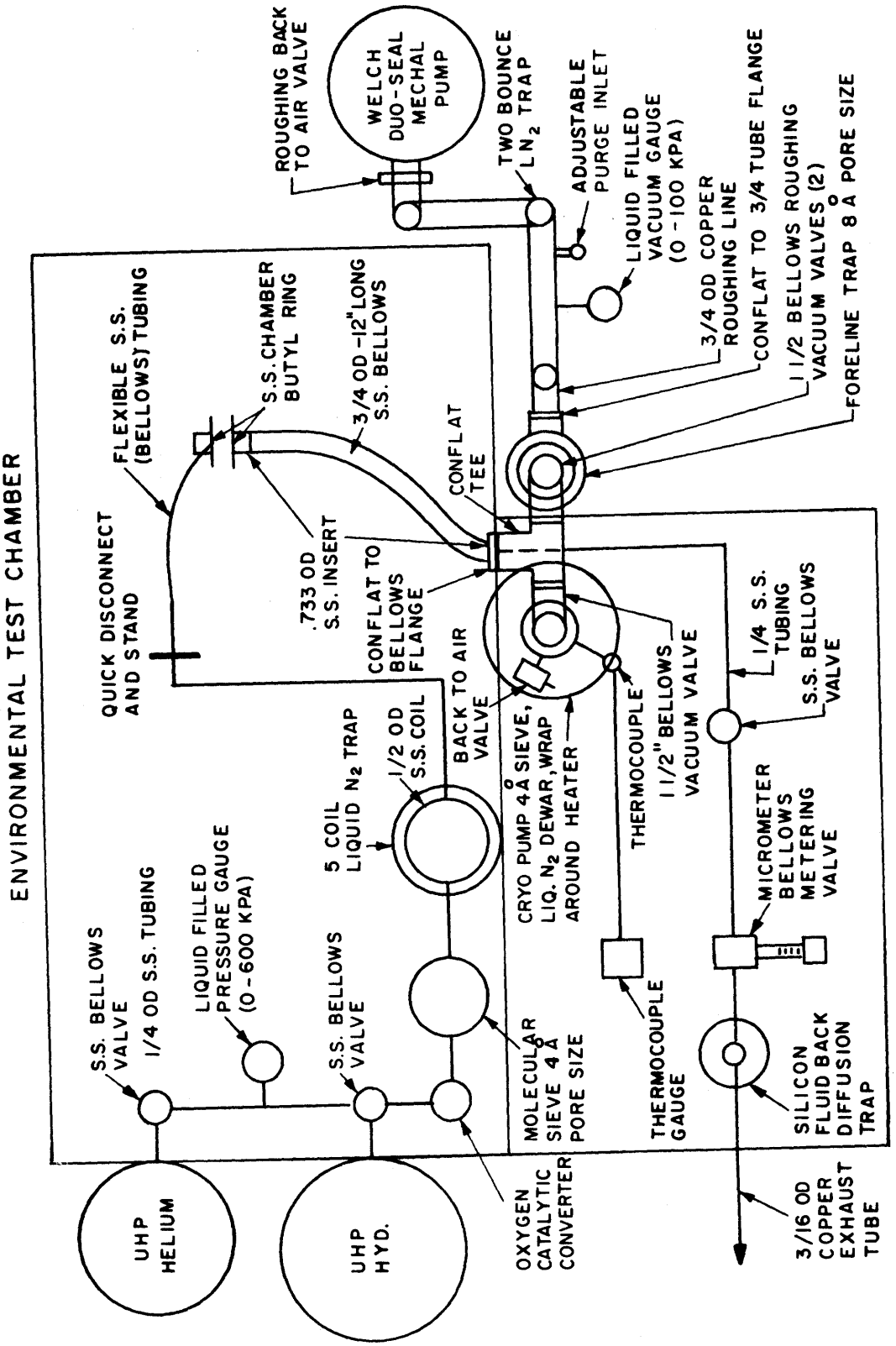

Fig. 32 Schematic representation of the environmental chamber system designed to produce an impurity level of less than 1 ppm.

4) Diffusion (flow through) of the test environment through a silicon fluid diffusion trap at a precise rate.

The system gas source consists of 99.999% UHP helium and 99.999% UHP hydrogen, each with rated impurity levels of less than 3ppm moisture, less than 1ppm oxygen and less than 0.5ppm hydrocarbons. Each gas flows through separate 316 stainless steel bellows vacuum valves into 6mm stainless steel seamless tubing. System gas then flows through an oxygen catalytic converter to react any oxygen present with hydrogen, producing water vapor. This moisture is then removed by an impurity adsorbing Matheson model 461 purifier, utilizing sodium alumino silicate 4 Å molecular sieve material. Final traces of moisture are then removed by passing the gas through a liquid nitrogen coil trap consisting of five coils of 316 stainless steel seamless tubing (fig. 33). A well designed trap should have a minimum impedance, a constant temperature at -196°C and a recommended inner surface area greater than 100 cm^2 for small vacuum systems (66). Therefore the coil tubing inner diameter was increased to 9.5mm to increase surface area (215 cm^2) and conductance.

Prior to entering the specimen chamber, the gas is passed through approximately one meter of tubing and bellows to return the gas temperature to ambient. This 316 stainless steel metal bellows, protected by braided wire sheath to allow for chamber motion, is connected to the inlet specimen chamber by inert shielded

Fig. 33 Rear view of the environment chamber system showing the liquid nitrogen coil trap, silicon fluid trap shield, roughing two bounce trap, and model 461 purifier.

gas arc welding (figs. 34 and 35).

The locally mounted chamber is made of 316 stainless steel and was designed using a semi-elliptical shape. The main design obstacle in this environmental chamber system was the sealing of the chamber on the face of the CT testpiece and across the notch. The list of alternative sealing methods was greatly reduced due to the fact that the stainless steel chamber had to be electrically insulated from the steel specimen. The most promising seal seemed to be an elastomer o-ring. Problems with this method were the need for a large squeeze of the ring so as to increase the sealing facial area. To provide this area a large circular cross section was needed, but this conflicted with the space requirements allowed. The problem was solved by designing a special lathe cut rectangular 'o-ring' of cross section 2.7mm x 5.4mm. This provided the added material upon compression to prevent metal contact and to reduce outgassing to an absolute minimum.

O-ring material design is a function of temperature range, pressure range, seal type and the working fluid used. The material used for this application has to withstand ambient to 100°C temperature, medium vacuum to pressures up to two atmospheres, and seal hydrogen. Farkass and Barry (63) performed tests on the base pressure attainable in a vacuum chamber using o-rings of various elastomers. Results showed that butyl produced the lowest pressure, and butyls outgassing was comparable to the

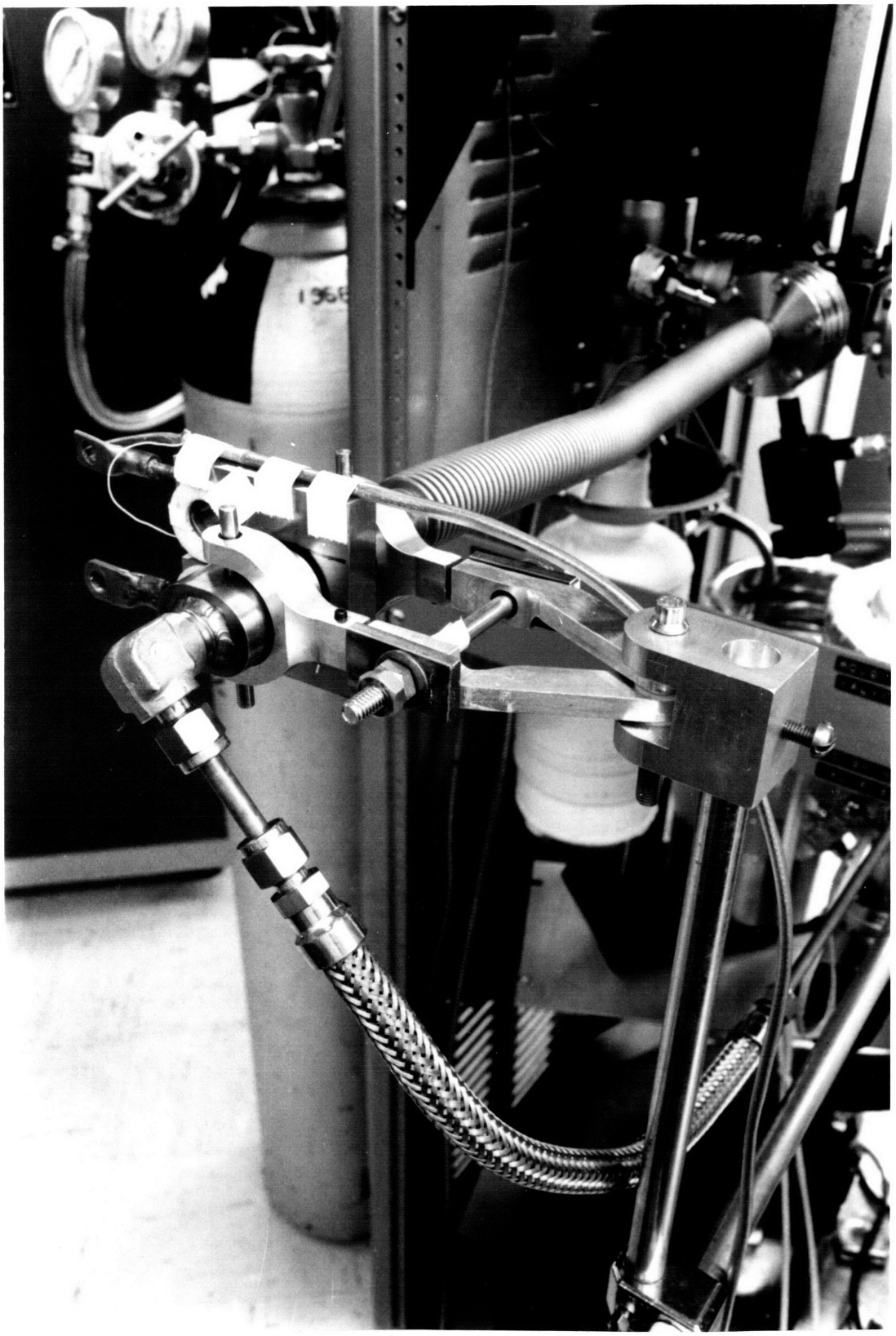

Fig. 34 Closeup view of the CT specimen mounted in the environment chamber showing the semi-elliptical chamber, yoke arms and mounting system.

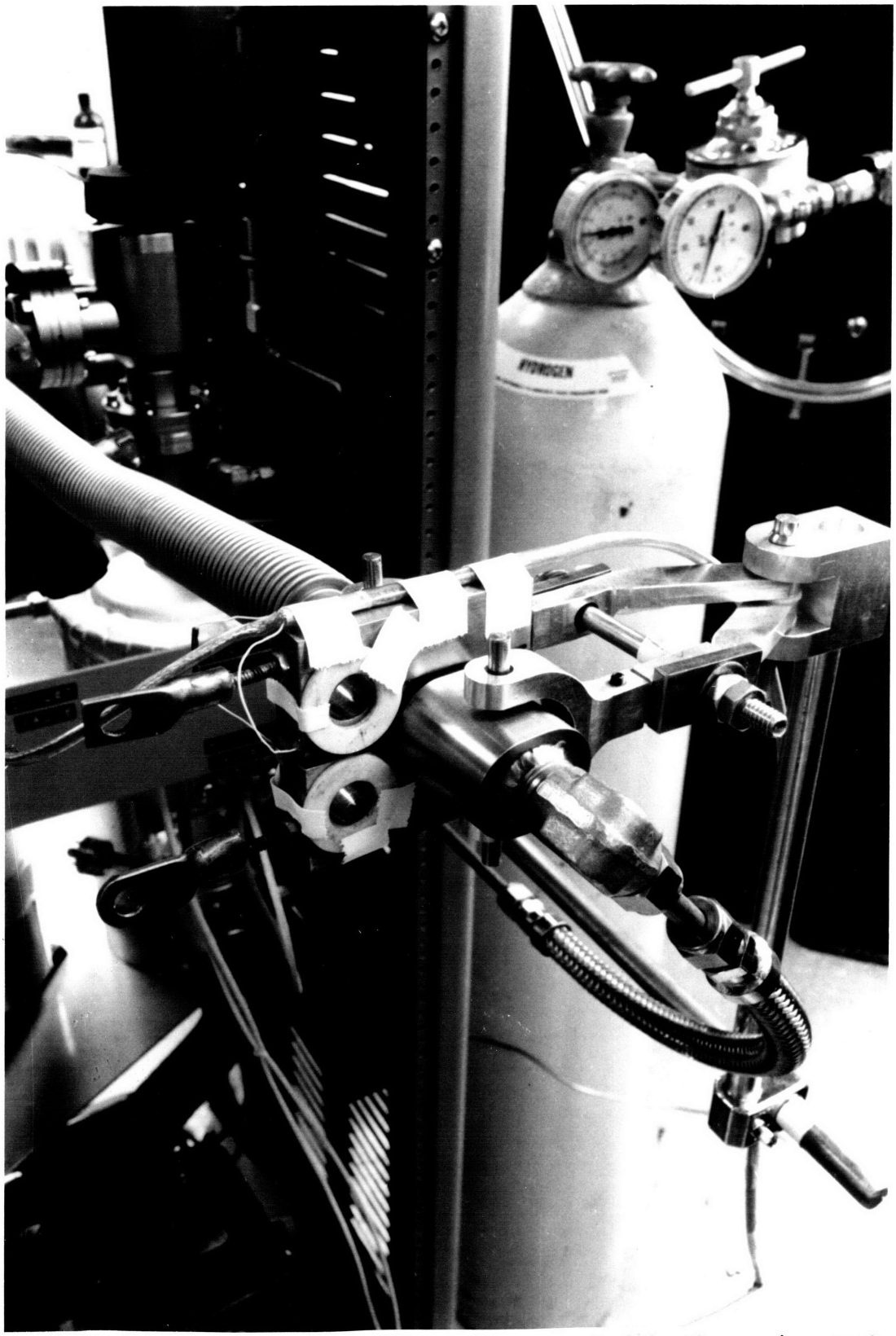

Fig. 35 Closeup view of the CT specimen mounted in the environment chamber showing the semi-elliptical chamber, yoke arms and mounting system.

best. Butyl rubber has been the preferred material for vacuum sealing applications (64). Checking an o-ring compatability list for hydrogen, gives butyl as the recommended material (64). Butyl also has good physical properties for a seal (compression set resistance) and good moisture resistance. For face seal applications, a material shore durometer hardness of 70 is recommended (64). Therefore, a butyl material was chosen with a shore value of 70. The design of the ring gland provides for a stretch fit. Stretch is recommended to not exceed 5%, therefore chamber design produces a 2% stretch. The gland is designed such that a 30% squeeze will leave a chamber/specimen clearance of 1mm.

To produce the required ring compression, two yoke shaped arms are connected to the chamber by press fit pins (fig. 34). Motion about these pins (by teflon inserts) allows automatic alignment of the chamber surface with the specimen surface. The yoke arm is connected to a back arm by a swivel pin which allows movement in yet another plane. Teflon washers are used for lubrication between the two arms. The arms have been designed for easy installation and removal. Sealing in the specimen notch is attained by utilizing a compressed section of butyl rubber.

The outlet chamber provides a large 19mm opening to which a 321 stainless steel bellows has been inert gas arc welded. The bellows provides a 20% compression and 50% extension from its original 30cm length to allow for motion in chamber

attachment. The outlet of the bellows is welded to a conflat tee (fig. 36). In addition to the outlet flow through line, two pumps are connected to this tee; a mechanical roughing pump and a cryogenic pump.

The Vacsorb cryogenic pump consists of an enclosure, refrigerated to liquid nitrogen temperatures, containing an activated sorbent. On opening the pump to the system, gas is adsorbed until the sorbent is saturated. Physical adsorption produces the pumping action, and the cryopump can attain relatively high pumping speeds. The final pressure achieved by sorption pumping can be improved by pre-pumping with a mechanical pump. The cyropump is a pump for residual impurities such as CO, CO_2, O_2, H_2O, N_2 and A (71).

Sorbent materials in commercial sorption pumps are the zeolites, known as 'molecular sieves'. Zeolites ability to adsorb large quantities of gases, rests on its unique porous crystal structure. The material has a series of molecular size cavities linked by molecular size openings or pores which are of constant and controllable dimensions. The molecular sieve possesses a large surface area to volume ratio of approximately 800 m^2/cm^3. Therefore, the cryopump used has nearly 300 acres of surface area. Pores in the material are 4 Å in diameter. After pumping down to the equilibrium pressure, the valve to the cryopump is closed and the molecular sieve is saturated. Normally warming the sieve to room temperature is all that is

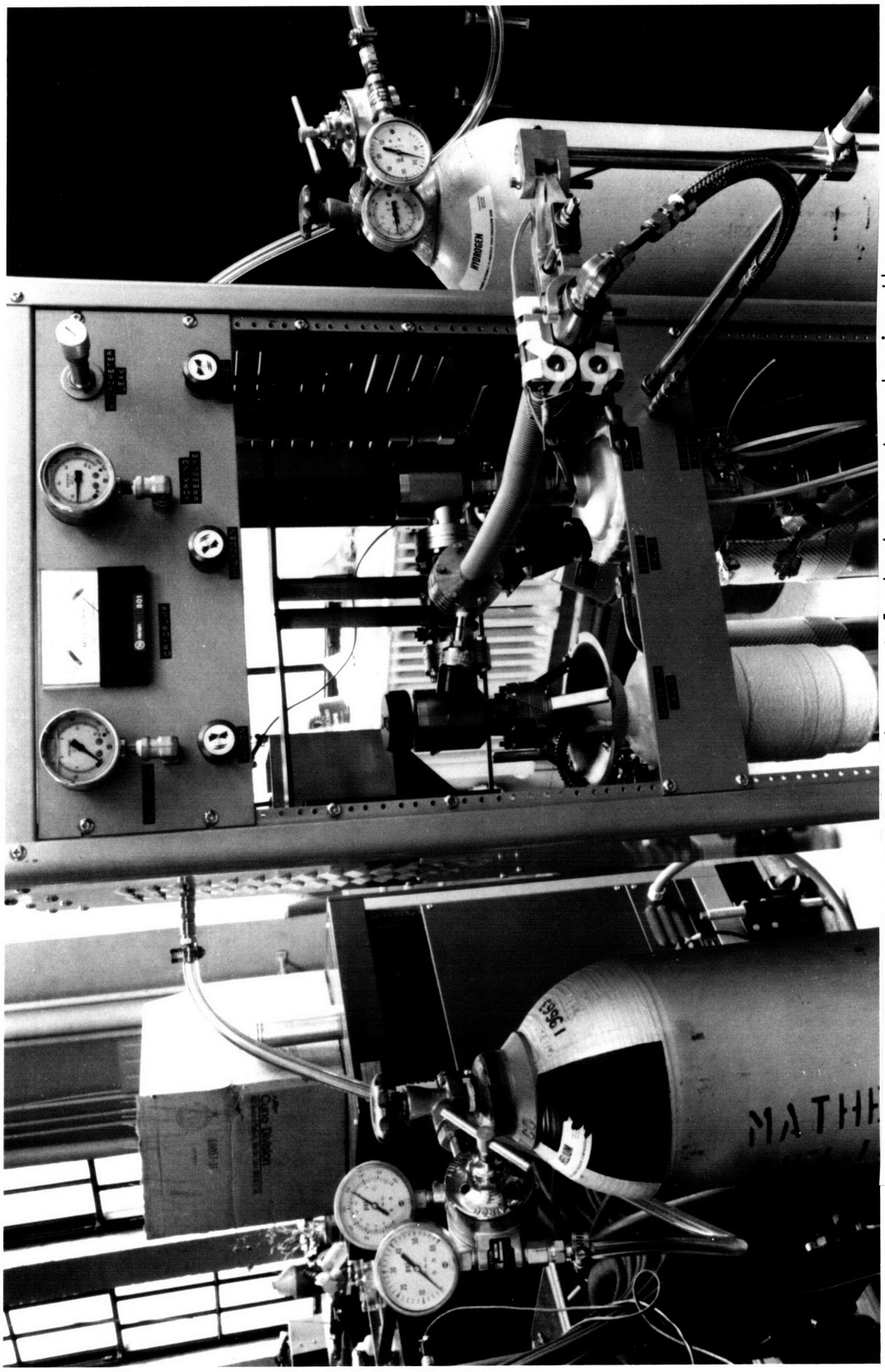

Fig. 36 Front view of the environmental chamber system showing the mounted CT specimen, outlet/inlet bellows, valves, cryopump, conflat tee and forelinetrap.

necessary to prepare for the next pump-down. However, adsorbed water is not readily evolved from the molecular sieve at room temperature. It is necessary to bake the sieve material by using a wrap around heater (fig. 33) that can heat to 300°C. The process of baking the molecular sieve is called activating.

The cryopump is isolated from the tee and the system by a high vacuum 1 1/2 inch viton sealed valve featuring 600 series Inconel bellows (bakeable to 200°C). The opposite end of the tee connects to the roughing line also by an Inconel bellows valve. A foreline trap, situated at the chamber side of the roughing line, is an extruded aluminum, internally finned body filled with 8 Å pore size molecular sieve (figs. 33 and 36). The trap protects the vacuum system (100% filtration) from back streaming of oil vapour from the mechanical pump, and also pumps water vapour to provide lower roughing pressures. The 8 Å pore size sieve material works on the same principles as the cryopump except that it operates at ambient temperature. Regeneration of the sieve material is performed by baking at 250°C for at least two hours to drive off water vapour and sorbed oil vapours.

The foreline trap is connected to a 19mm copper tube roughing line by brazing. This roughing line runs to a Welch Duo Seal model 1402 mechanical pump, of pumping speed 140 liters per minute. The roughing line features a liquid nitrogen cooled two bounce trap (fig. 33). This trap is in operation whenever the system is pumping to help prevent backstreaming of oil (75).

Additional means of preventing hydrocarbon contamination involved inserting an adjustable purge inlet in the roughing line just before the mechanical pump. An adjustable purge inlet allows air to escape into the roughing pump if flow leaves the viscous flow regime. A back to air valve is used to bring the roughing line and pump pressure back to atmospheric, once pumping has ceased.

An exhaust flow through line of 6mm stainless steel tubing originates from an outlet valve connected to the conflat tee. This line runs to a stainless steel metering bellows valve (fig. 36) featuring a micrometer adjustment handle for setting precise flow rates. Flow through this line will filter into a silicon fluid back diffusion trap (fig. 33), then be released to the environment through approximately 15m of 1.5mm inner diameter copper tubing. The tubing size is required so that possible ignition of hydrogen at the final outlet will not travel back to the system. The flow rate will be set at approximately 5 cm^3/min. A flow through system allows a fresh environment to be maintained at the fatigue crack front.

The most effecient method of reducing the outgassing rates of the parts of the vacuum system is their baking. Water vapour, hydrogen, carbon monoxide, carbon dioxide, oxygen and nitrogen are commonly evolved gases on baking metals in vacuum or under an inert purge. Therefore, the chamber system procedure allows for baking of most of its components.

This system has been designed primarily for ambient temperature testing in UHP hydrogen and helium at pressures under 200 kPa (2 Atms). Chamber system design permits adaptation for installing a mass spectrometer if desired to separate gases present according to their mass to charge ratio.

System Procedure

The CT specimen is initially polished and cleaned. The notch seal is inserted and edges are shaved. After electrical leads and ceramic washers are attached (fig. 35), the specimen is critically positioned in the chamber. Valves are closed in the system such that it leaves only the gas input lines, specimen chamber, bellows, tee and outlet line as the main chamber enclosure (fig. 32). The system is then pressurized with helium, and allowed to flow through at a set rate. The main chamber is then baked at approximately 100°C. While baking the chamber, the foreline trap is baked for two hours while under vacuum. The two bounce trap is then filled with liquid nitrogen while the system pressure is allowed to reduce to atmospheric. The chamber enclosure is then evacuated by the roughing system until a minimum pressure is attained. During these past steps, the cryopump has been baked for 3 1/2 hours, cooled to ambient, and then taken to liquid nitrogen temperature. The roughing system is then sealed off and the cryopump opened to the chamber. Once a minimum system pressure is attained, the cryopump is sealed off. The liquid

nitrogen coil trap is cooled to -196°C, and the system is then pressurized to 16 psig with the UHP test gas. This procedure of 'cleaning' the chamber takes about eight hours. The CT specimen and chamber is now ready to be mounted in the testing machine.

APPENDIX B

FATIGUE TEST RESULTS: 320°C TEMPER

Tempering at 320°C produced test results believed to be strongly influenced by residual stresses still present from the vigorous quench from austenitization. Therefore, two subsequent heat treatment procedures were attempted. The second treatment (320°C (II)) involved austenitizing/quenching and tempering/quenching a specimen blank (without CT notch or loading pin holes). This condition also produced test results believed to indicate a large degree of residual stresses present. The third treatment (320°C (III)) involved full heat treating of a large plate (1 in x 6 in x 9 in), following by machining of the test pieces. Due to the size of this plate, an endothermic atmosphere furnace had to be used which allows the carbon content to be set according to material content, to prevent decarburization. This 320°C (III) condition still produced mostly questionable test results, but was significantly improved over the first two treatments. It is understood that material properties could vary between these 320°C temper treatments. However, it is believed that the critical cooling velocity was attained in each case (fig. 37) so as to produce the quenched condition initially desired. It is also understood that tempering a quenched material at this temperature (320°C) is not recommended in applications due to the large loss of ductility. The reason for testing the 320°C temper was due

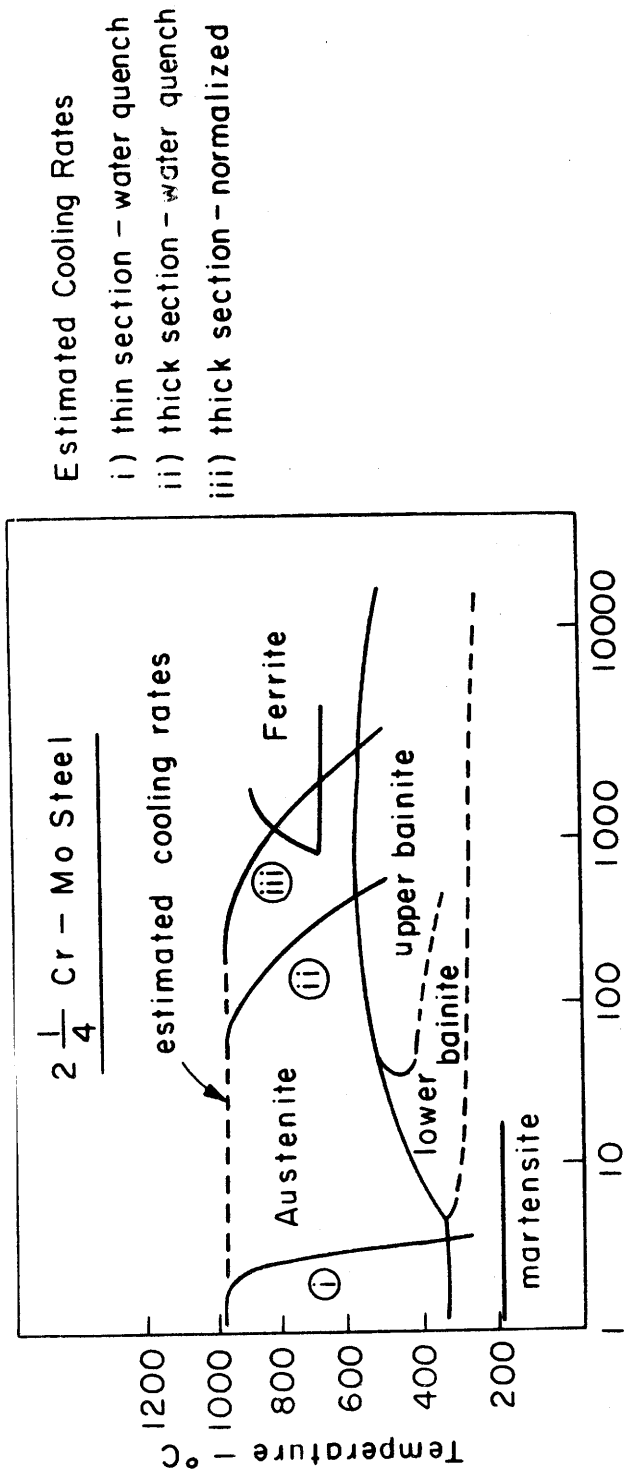

Fig. 37 Schematic continuous – cooling transformation diagram for $2\frac{1}{4}$ Cr – 1 Mo Steel

to the high yield strength produced (951 MPa).

Near-threshold crack growth tests for the 320°C temper condition produced results that were believed to be affected by residual stresses. The results obtained improved on going from method I to method III, but all tests except two (from the third method) produced crack fronts that included multiple initiation and propagation or exaggerated tunnelling. In the latter, the crack center was observed to grow by as much as 12 mm ahead of the crack sides (in a 12 mm thick specimen). The results are inaccurate when using the electrical potential method to measure a growing crack through a CT specimen. Figure 38 displays crack fronts experienced in testing the 320°C temper. Figure 38a exhibits initiation at three points along the notch, with the right side growing approximately five times the center site, and two times the left site in distance once the threshold ΔK_o was reached. Crack front tunnelling (fig. 38b) was experienced in the majority of the invalid tests. It was attempted to alleviate this problem by machining off varying amounts of material off each specimen face. In each case, either the tunnelling effect reoccurred or the crack front grew in an asymmetrical fashion.

Hardness profiles were taken across the specimen thicknesses of all three treatment conditions. An average variation of 5% was found from a maximum in the center to a minimum along both sides. This experiment seems to be only a start into analyzing

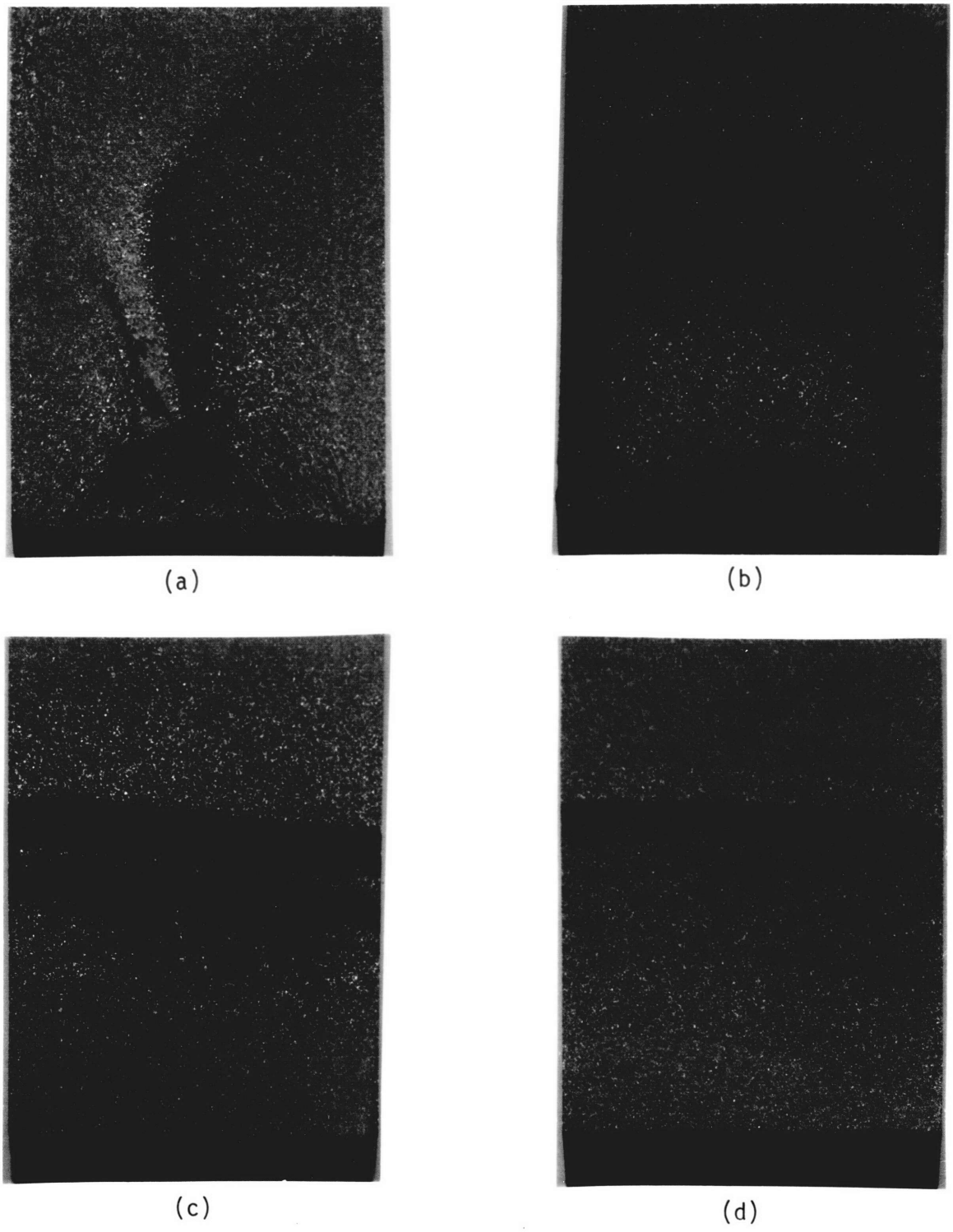

Fig. 38: Closeup view of CT testpiece crack fronts encountered in testing the 320°C temper condition (a) multiple initiation (b) tunnelling (c) valid test in air (d) valid test in hydrogen (4 1/2 X).

this problem. Future work is needed to further examine this test condition.

The two tests that did produce straight cracks (fig. 38c and 38d) are plotted in figure 39. It is seen that for low R, the hydrogen environment did lower the threshold ΔK_o from 7.6 MPa $\sqrt{m}$ for moist air to 6.0 MPa $\sqrt{m}$. The value of 7.6 MPa $\sqrt{m}$ for moist air does not fit the trend of yield strength tests as seen in figure 7. Therefore, it is not known whether these results are accurate or if they are affected by possible residual stresses. Specimens from the 470°C and 550°C temper conditions were tested to provide a third data point for the strength effect. However, the few tests attempted, also produced questionable crack fronts. Future work is needed to fulfill the material strength effect for the SA542 class 2 steel.

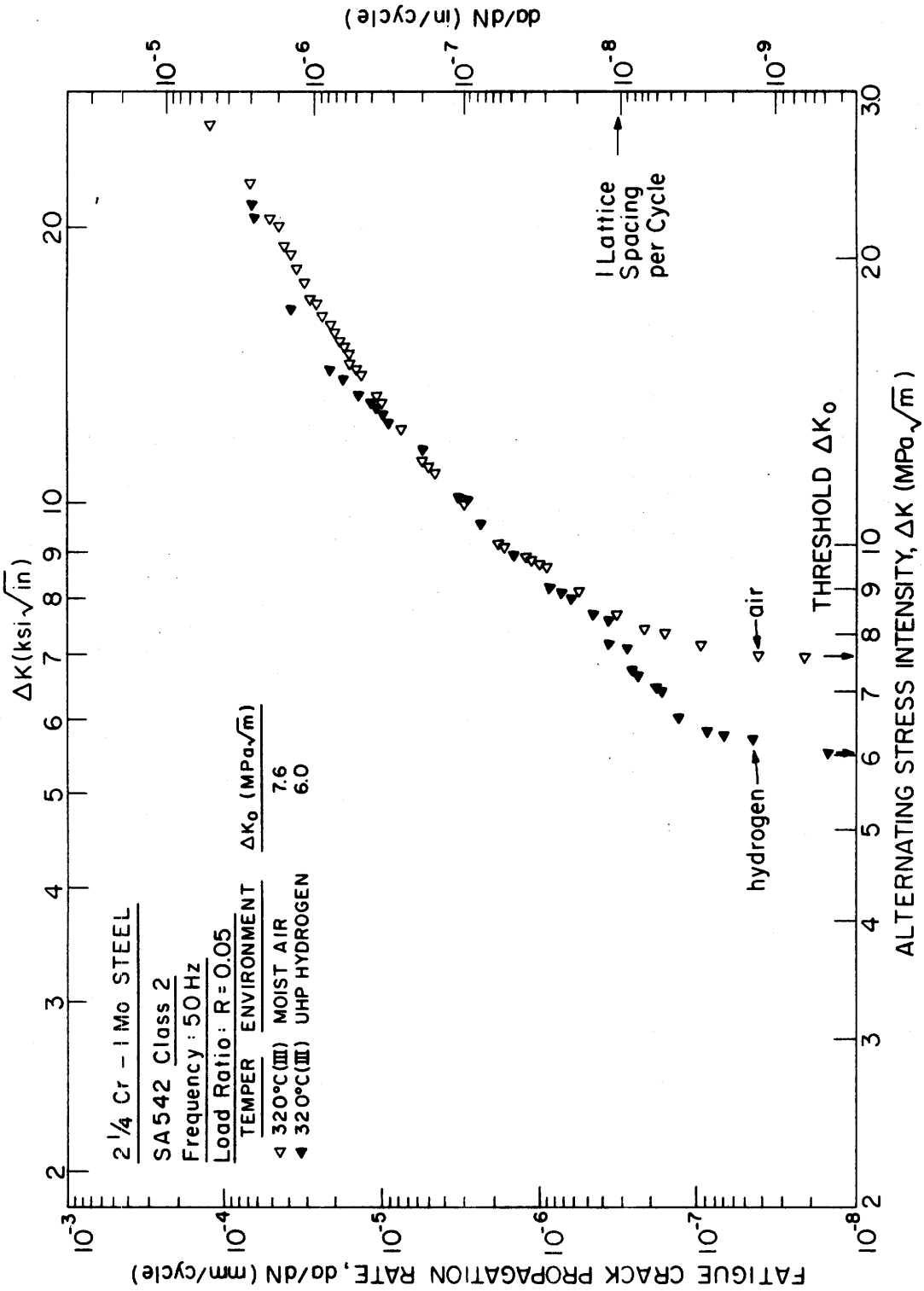

Fig. 39 Fatigue crack growth data for the 320°C (III) temper at R = 0.05 in moist air and UHP hydrogen.